Synthesis, Characterization, and Biophysical Interaction Studies of Water Soluble Polypyrrole/Polythiophene Co-oligomers with Bovine Serum Albumin and Human Serum albumin: An Experimental and Theoretical Approach

Journal:	*New Journal of Chemistry*
Manuscript ID	NJ-ART-11-2022-005791.R1
Article Type:	Paper
Date Submitted by the Author:	23-Dec-2022

Complete List of Authors:	Riaz, Ufana; Jamia Millia Islamia, Chemistry farooq, aaliyah; Jamia Millia Islamia, Chemistry Mir, Nuzhat; Materials Research Laboratory, ; Jamia Millia Islamia, Department of Chemistry Nwanze, faith ; North Carolina Central University, chemistry yang, fei; North Carolina Central University, chemistry

Synthesis, Characterization, and Biophysical Interaction Studies of Water-Dispersible Polypyrrole/Polythiophene Co-oligomers with Bovine Serum Albumin and Human Serum albumin: An Experimental and Theoretical Approach

Ufana Riaz [a,b*] ,Aaliyah Farooq[b], Nuzhat Mir[b], Faith R Nwanze[a] and Fei Yan[a]
[a]Department of Chemistry and Biochemistry, North Carolina Central University, NC, 27707, USA
[b]Materials Research Laboratory, Department of Chemistry, Jamia Millia Islamia, New Delhi 110025, India, *Corresponding author: Fax-(+91-112-684-0229); E-mail address-(ufana2002@yahoo.co.in)

Abstract

The present work reports the synthesis of water-dispersible polypyrrole (WD-PPy) and polythiophene (WD-PTh) copolymers in different weight ratios and their characterization using experimental as well as theoretical techniques. The copolymers were spectroscopically characterized using experimental ^{13}C-NMR, FTIR, UV-visible, and theoretical FTIR, UV-visible studies. The theoretical frequency, as well as UV-visible data, were computed using Gaussian 09 software with functional DFT/B3LYP method and 6-31G (d) basis set. For the first time, biophysical interaction studies were carried out using bovine serum albumin (BSA) and human serum albumin (HSA) for these polymers which are not yet reported in the literature. Results showed strong binding of the co-oligomers with BSA/HSA which could be utilized in designing potent inhibitors and biosensors.

Introduction

Electroactive polymers such as polyaniline (PANI) [1], polypyrrole (PPy) [2], polythiophene (PTh) [3], poly(o-phenylenediamine) (POPD) [4], poly(1-naphthylamine) (PNA) [5], polycarbazole (PCz) [6] have been utilized in diverse applications such as biosensors [7], supercapacitors [8] battery electrodes9, photocatalysts [10], microbial fuel cells [11] etc. Among all, PPy and PTh display exceptional properties such as ease of preparation, good redox behavior, high electrical conductivity, and good thermal stability [12-13]. The achievement of high conductivity is mainly due to the positive charge generated on the backbone of these polymers particularly when polymerized using $FeCl_3$ as oxidant which also acts as dopant anion. However, most of the chemical and electrochemical techniques used for polymerization lead to the production of insoluble and intractable forms [14-15].

Chemical polymerization is a facile technique to synthesize water soluble conducting polymers via the incorporation of flexible side chains which can solubilize in organic solvents. *Masuda and Kaeriyanma* [16] reported the synthesis of water-soluble conducting polymers using sodium salt of poly(thiophene-3-carboxylate). *Lu et al*. [17] reported the synthesis of PPy by interfacial polymerization at the interface of chloroform (with monomer) and water (with dopant/oxidizing agent) solutions. *Heeger et al.* [18] reported the synthesis of the sodium salts and corresponding acids of poly(thiophene ethane sulfonate) and poly(thiophene butane sulfonate). Wang and coworkers [19] synthesized a water-soluble polythiophene derivative with tyrosine kinase inhibitor *lapatinib* as pendant moieties, utilized for imaging of living cells.

Water solubility of conducting polymers provides a versatile platform for sensing of various chemical and biological species due to the unique light-harvesting ability of these polymers. Fluorescence imaging and real-time sensing capacities demonstrate rapid and highly sensitive detection of various proteins such as bovine serum albumin (BSA) and human serum albumin the via selective binding which are used to diagnose diseases/ formulate several kinds of drugs. The ability of conducting polymers to act as a platform for protein-surface interactions and to covalently attach functional groups that provide protein binding sites has lately found immense application in the area of biosensors and for controlled cellular interactions [20].

Keeping this in mind, we have developed water-dispersible PPy (WD-PPy), water-dispersible PTh (WD-PTh), and a series of copolymers of WD-PPy/WD-PTh via interfacial polymerization method using different loadings of the monomers. Interfacial polymerization has been used by authors to develop water-dispersible conducting polymers [21-22]. The homo-oligomers as well as co-oligomers revealed high water solubility and were characterized using ^{1}H-NMR ^{13}C-NMR, FTIR, UV-visible, SEM analyses. The theoretical studies of these polymers were also computed via Gaussian 09 software using B3LYP functional and 631G (d) basis sets. BSA and HSA were used as model proteins to explore the protein-polymer interactions due to their structural similarity, low cost, ease of purification, and the ability to produce fluorescence emission. The interactions were investigated by UV-visible and docking studies.

Experimental

Pyrrole (Sigma Aldrich, USA), thiophene (Sigma Aldrich, USA), ferric chloride (Merck, India), dimethyl sulphoxide (DMSO) (Merck, India), and deionized distilled water were used without further purification.

Synthesis of water dispersible polypyrrole (WD-PPy)

A mixture of distilled water (40 ml) and DMSO (10 ml) was taken in a round bottom flask and pyrrole monomer (8 ml, 0.11 mol) was added to the above mixture which was subjected to sonication on an ultrasonic bath 30 ^{o}C equipped with a thermometer and nitrogen inlet. The mixing was carried out for around 2 h. $FeCl_3$ (3 g, 0.01 mol) was then added drop-wise to the above solution and the color of the solution turned black indicating onset of polymerization. The polymerization was allowed to continue for 24 h at 30^{o}C. The black precipitates obtained were filtered and washed with H_2O and ethanol to remove the traces of oxidant from the synthesized product. The precipitate was dried in a vacuum oven at 60 ^oC for 24 h.

Synthesis of water dispersible polythiophene (WD-PTh)

Thiophene monomer (8 ml, 0.09 mol) was dissolved in chloroform (50 ml) in a 250 ml conical flask and was sonicated on an ultrasonic bath for about 4 h. $FeCl_3$ (3 g, 0.01 mol) dissolved in water (10 Ml) was then added dropwise to the thiophene solution and the mixture was sonicated for 24 h at 30 ^oC. The obtained precipitate of the polymer was filtered and washed with de-ionized water to remove the unreacted monomer, traces of oxidant and other impurities. The filtrate was finally dried in a vacuum oven at 60 °C for 24 h.

Synthesis of water dispersible pyrrole/thiophene copolymers (WD-PPy/PTh)

Deionized distilled water (30 ml), DMSO (10 ml) and chloroform ((10 ml) in a 250 ml conical flask and monomer of pyrrole (4 ml, 0.05 mol) thiophene (4 ml, 0.05 mol) were added and sonicated on an ultrasonic bath for 4 h. $FeCl_3$ (3g, 0.01 mol) was added dropwise to the mixture of pyrrole/thiophene solution and sonicated for 24 h at 30 °C on an ultrasonic bath. The obtained copolymers were then filtered and washed with deionized water, and ethanol to remove the unreacted monomer, oxidant and other impurities. The filtrate was finally dried in a vacuum oven at 80 °C for 24 h. The copolymer was designated as WD-PPy/PTh-1/1. Similar procedure was adopted for the synthesized of WD-PPy/PTh taking the mol ratios to be 4:1 and 1:4 which were designated as WD-PPy/PTh-4/1 and WD-PPy/PTh-1/4. The viscosity average molar mass of the synthesized polymers was determined as per method reported in our earlier studies and was computed to be 3587 for WD-PPy, 4523 for WD-PTh, 5438 for WD-PPy/PTh-4/1, 4898 for

WD-PPy/PTh-1/1 and 5804 WD-PPy/PTh-1/4 [23]. Hence the polymers were designated as oligomers and co-oligomers.

CHARACTERIZATION

Spectral studies

IR spectra of co-oligomers were taken on FT-IR spectrophotometer model IRA Affinity-1 in the form of KBr pellet. UV-Vis spectra were taken on UV-Vis spectrophotometer model Shimadzu UV-1800 using water as a solvent. UV measurements were recorded using optical path lengths ranging between 1.0 and 10^{-2} cm for solutions. ^{1}H-NMR spectra were recorded at 25 °C on a Bruker 300 MHz spectrometer using deuterated dimethyl sulphoxide (DMSO) as solvent. a fresh homogeneous solution was prepared of 50 mg of the oligomers in 0.5 ml of DMSO. The solutions were spiked with trimethylsilane (TMS) and analyzed in sealed 5 mm quartz NMR tubes with a spin speed of 20 Hz.

Gaussian calculations

The geometries were optimized at the B3LYP functional level using a 6-31G (d) basis set [23]. The oscillator strength, highest occupied molecular orbital (HOMO) and lowest unoccupied molecular orbital (LUMO) energies, and band gap was determined using the optimized geometries with the same basis set. The vibrational frequencies were computed using the same basis set. The UV spectra were of optimized geometric structures were simulated at TD-DFT/ B3LYP using 6-31G (d) basis set [23].

Biophysical interaction studies

Interaction of synthesized water dispersible polymers with bovine serum albumin (BSA) and human serum albumin (HSA) was studied via UV–vis spectroscopy in buffer solution to explore the change in absorbance of the biological macromolecules upon interaction with polymers as per method reported in our earlier studies [24]. The quantitative binding affinity of was analyzed by the Benesi-Hildebrand equation as mentioned in literature [25].

Docking studies

Molecular docking was performed using Auto Dock Vina program [26]. The three dimensional crystal structures of BSA and HSA were downloaded from RCSB Protein Data Bank in pdb format. The water molecules surrounding BSA, HSA were removed and Kollman charges were added after merging all the non-polar hydrogen atoms. The coordinate file of BSA, HSA was then saved into PDBQT. The size of the grid was set to 80 × 60 × 86Å with maximum spacing of 1Å to cover all the active sites in BSA and HSA with center of the grid at x = 29.535, y = 31.826 and z = 23.5. Structure of oligomers was converted to pdb format and post modelling analysis was done using Discovery Studio 2016 and PyMol. The docked conformation with the lowest energy was selected for analysis [25-26].

Results and Discussion

The conducting polymers synthesized via interfacial polymerization are reported to show solubility in different solvents and dispensability in water as shown in Table S1 (provided in supplementary information) [21-22]. WD-PTh and WD-PPy showed uniform morphology as discussed in SEM in the proceeding section. The interaction between the organic solvents used in interfacial polymerization play an important role in enhancing the miscibility of WD-PPy and WD-PTh in water as the monomer is soluble in the organic solvent while the initiator (ferric chloride) is soluble in the water medium. It has been reported that $FeCl_3$ exhibits good solubility in organic solvents as well as water and can lower the oxidation potential of thiophene to accelerate polymerization and likely form an oligomer. Hence it can be concluded that interfacial polymerization in our case leads to the formation of oligomers of WD-PTh and WD-PPy due to which they show dispersibility in water.

Morphological Studies

The SEM of WD-PPy, Figure 1(a), exhibited a granular morphology and the particles appeared to be scattered as tiny grains. The SEM of WD-PTh, Figure 1(b), showed bright dense spherical clusters. The SEM of WD-PPy/PTh-4/1, Figure 1(c), showed a predominance of PPy morphology (loading was higher) with the appearance of bright PTh particles as agglomerates. The SEM of WD-PPy/PTh-1/1, Figure 1(d), showed a granular morphology with uniform distribution of PPy/PTh particles that appeared to be well-interconnected. The SEM of WD-PPy/PTh-1/4, Figure 1(e), revealed flaky particles of PTh forming dense granular agglomerates. The predominance of WD-PPy showing dull granular morphology was noticed in WD-PPy/PTh-4/1, while a predominance of WD-PTh morphology showing bright clusters of white particles was observed in WD-PPy/PTh-1/4. A mixed morphology was noticed in WD-PPy/PTh-1/1. The SEM studies clearly reflected the variation in the morphology upon loading of PPy and PTh at various concentrations.

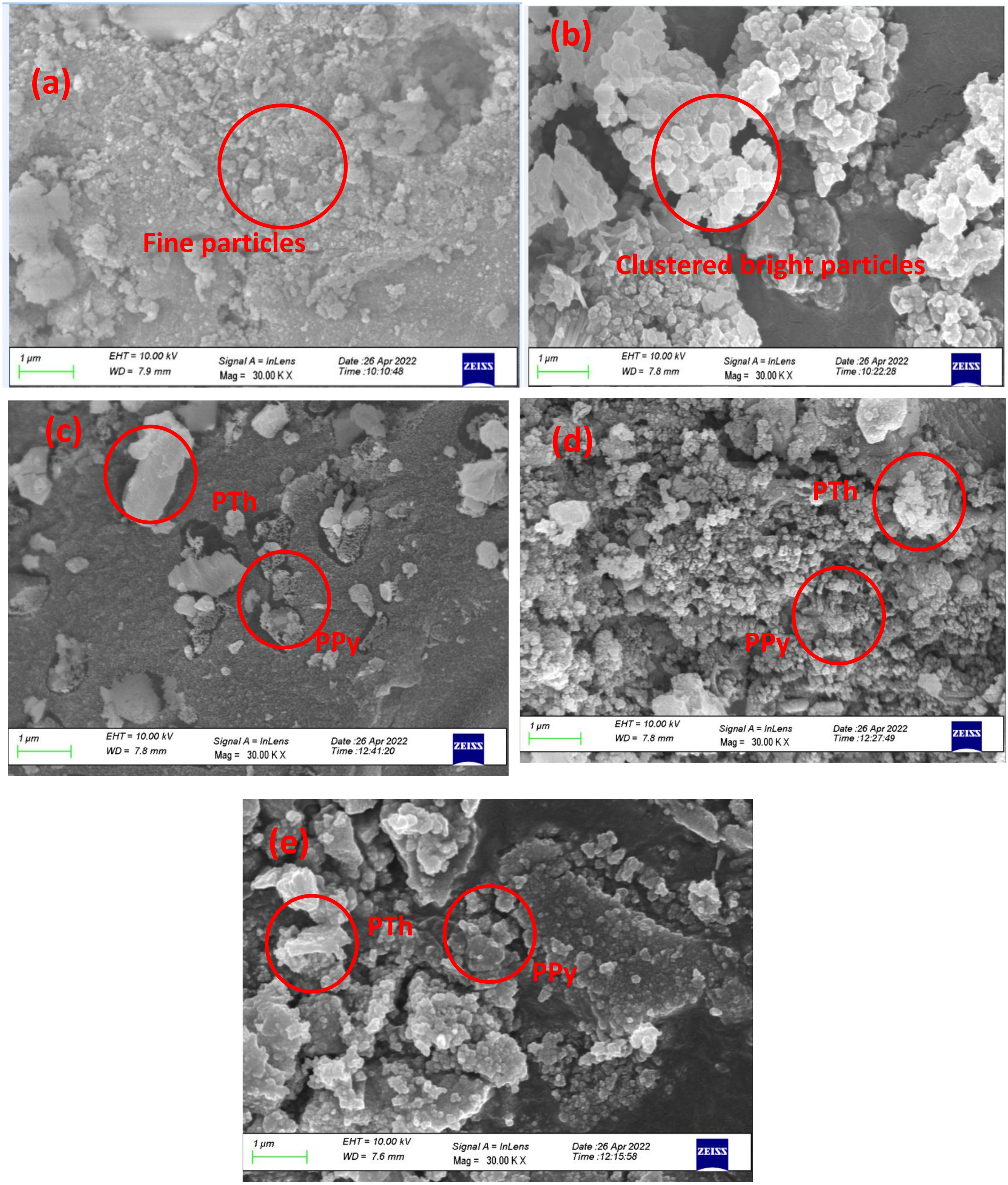
(a)
Fine particles
1 µm
EHT = 10.00 kV
WD = 7.9 mm
Signal A = InLens
Mag = 30.00 K X
Date :26 Apr 2022
Time :10:10:48
ZEISS
(b)
Clustered bright particles
1 µm
EHT = 10.00 kV
WD = 7.8 mm
Signal A = InLens
Mag = 30.00 K X
Date :26 Apr 2022
Time :10:22:28
ZEISS
(c)
PTh
PPy
1 µm
EHT = 10.00 kV
WD = 7.8 mm
Signal A = InLens
Mag = 30.00 K X
Date :26 Apr 2022
Time :12:41:20
ZEISS
(d)
PTh
PPy
1 µm
EHT = 10.00 kV
WD = 7.8 mm
Signal A = InLens
Mag = 30.00 K X
Date :26 Apr 2022
Time :12:27:49
ZEISS
(e)
PTh
PPy
1 µm
EHT = 10.00 kV
WD = 7.6 mm
Signal A = InLens
Mag = 30.00 K X
Date :26 Apr 2022
Time :12:15:58
ZEISS

Figure 1 SEM of (a) WD-PPy, (b) WD-PTh, (c) WD-PPy/PTh-4/1, (d) WD-PPy/PTh-1/1, (e) WD-PPy/PTh-1/4

Confirmation of polymer structures via ^{1}H-NMR and IR studies

The ^{1}H-NMR spectrum of WD-PPy (given in supporting information as Figure S1(a)), revealed a sharp peak at δ = 8.3 ppm of NH protons of pyrrole [24]. The heterocyclic ring protons of adjacent to the NH group appeared at δ = 7.3 ppm and δ = 7.6 ppm. The ^{1}H-NMR spectrum of WD-PTh (given in supporting in formation as S1(b)), exhibited a doublet peak at δ = 7.2 ppm and δ = 7.4 ppm corresponding to the protons of the heterocyclic ring of PTh. The ^{1}H-NMR spectrum of WD-PPy/PTh-1/1 (given in supporting in formation as S1(c)), showed 2 broad humps at δ = 6.8 ppm and δ = 7.9 ppm correlated to the heterocyclic ring protons of PPy/PTh as well as NH proton of pyyrole ring respectively. The peaks appeared to be broad and diffused due to the incorporation PTh in PPy and vice versa. The broadness of the humps was even related to hydrogen bonding with the solvent (DMSO) . The ^{13}C-NMR spectrum of WD-PPy (given in supporting information as Figure S2(a)), revealed a sharp peak at δ = 112 ppm corresponding to protonated carbons in pyrrole ring (b) [25-27]. The peak around 128 ppm was correlated to the protonated carbon (a) adjacent to the NH group, while the peak at 117 ppm was correlated to unprotonated carbons (c) [27]. The ^{13}C-NMR spectrum of WD-PTh (given in supporting in formation as S2(b)), exhibited peaks at δ = 113 ppm and δ = 117 ppm corresponding to the protonated carbons and unprotonated carbons of the heterocyclic ring of PTh respectively [28]. The peak at 129 ppm was associated with the unprotonated carbons adjacent to the S group of thiophene, The ^{13}C-NMR spectrum of WD-PPy/PTh-1/1 (given in supporting in formation as S1(c)), showed peak at δ = 109 ppm ,117 ppm 128 ppm, 130 ppm correlated to the protonated carbons of WD-PPy and WD-PTh respectively [29]. The peaks of the homo-oligomers showed a slight shift indicating the formation of block copolymers as shown in Scheme 1. For alternate copolymer several peaks would have appeared in the spectrum due to alternate linkages but the neatness as well as appearance of the peaks corresponding to the homo oligomers clearly reveals formation of block copolymer as shown in Scheme .1

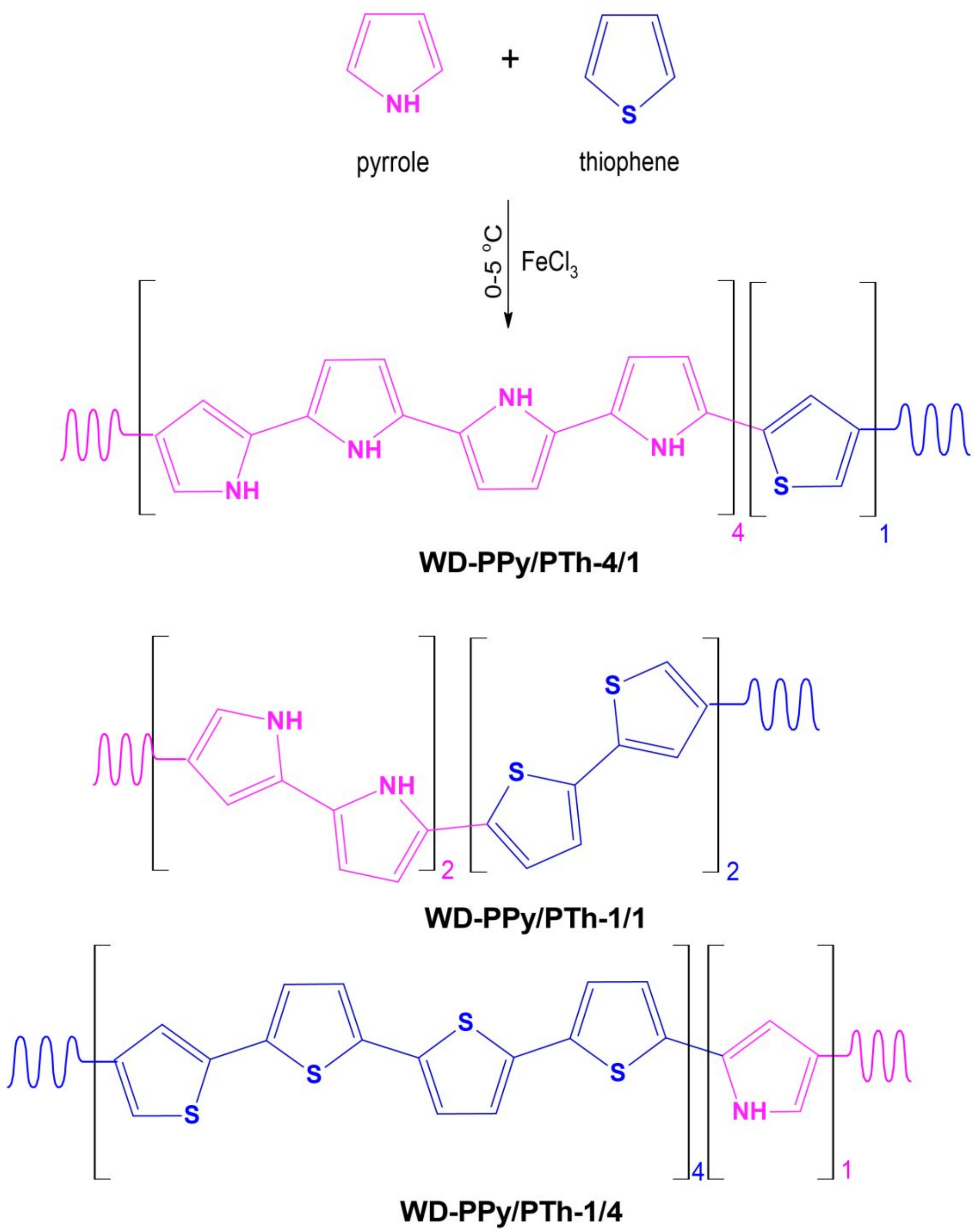

Scheme 1 Copolymerization of WD-PPy with WD-PTh

Based on the synthesis technique we have used; it is very unlikely that an alternate copolymer can be formed. The reactivity ratios of pyrrole and thiophene show the tendency to homo-polymerize and form short chains which subsequently react with the other monomers or oligomeric chains to form copolymers. The chemical oxidant polymerization utlilizes a strong oxidant which leads to quick radical generation in monomers and fast polymerization forming oligomers instantly. As far as computational studies are concerned, we tried correlating the experimental FTIR, and UV visible with the theoretical data generated by combining alternate and random sequences. The theoretical IR and UV-visible did not match our experimental data except in the case of block sequence that we used**.** The theoretical, as well as experimental FTIR studies, were carried out to confirm the geometry-optimized structures utilized for determining the band gap as well as the electronic transitions. The FT-IR spectrum of WD-PPy (provided in supplementary information as Figure S3(a)), Table 1, showed absorption peaks at 3488 cm^{-1} corresponding to NH deformation. The theoretical spectrum displayed the same peaks at 3616 and 3476 cm^{-1}. The peaks at 1605 cm^{-1} and 1045 cm^{-1} were correlated to the C=N stretching and were noticed at 1588 cm^{-1} and 1048 cm^{-1} in the theoretical spectrum of PPy. The C=C stretching peaks were found at 1441 cm^{-1} ,1409 cm^{-1} and 1323 cm^{-1}, while the theoretical spectrum showed the same peaks at 1450 cm^{-1},1408 cm^{-1}, and 1343 cm^{-1}. The C-C stretching vibration peak appeared at 1211 cm^{-1},1142 cm^{-1},1018 cm^{-1} , while the peaks at 842 cm^{-1}, 760 cm^{-1}, 699 cm^{-1} were associated with pyrrole ring deformations. The theoretical spectrum revealed these peaks at 1210 cm^{-1}, 1140 cm^{-1},1020 cm^{-1}, 840 cm^{-1},768 cm^{-1}, and 688 cm^{-1} respectively. The peaks confirmed the polymerization of pyrrole as reported by other authors [29].

The IR spectrum of WD-PTh, (provided in supplementary information as Figure S3(b)), Table 1, showed OH stretching vibration at 3424 cm^{-1}, while the theoretical spectrum revealed the same vibrations at 3445 cm^{-1},3250 cm^{-1}. The C=C stretching vibration peak was noticed at 1523 cm^{-1}, 1424 cm^{-1} ,1409 cm^{-1} ,1323 cm^{-1} and the theoretical spectrum showed the same peak at 1524 cm^{-1} ,1430 cm^{-1} ,1400 cm^{-1} ,1320 cm^{-1} . The C-S-C stretching peak appeared at 1021 cm^{-1},1019 cm^{-1} in the experimental spectrum and at 1130 cm^{-1},1010 cm^{-1} in the theoretical spectrum. . The peaks at 952 cm^{-1},908 cm^{-1},701, cm^{-1} were correlated to the presence of thiophene ring and confirmed the polymerization [19,29].

Table 1 IR spectral data of WD-PPy, WD-PTh, WD-PPy/PTh-4/1 WD-PPy/PTh-1/1 and WD-PPy/PTh-1/4

Polymer	Functional Group	Peak Position (cm^{-1})	
		Experimental	Theoretical
WD-PPy	NH deformation	3488	3616,3476
	C=N stretching	1605,1045	1588,1048
	C=C stretching	1441,1409,1323	1450,1408,1343
	C-C stretching	1211,1142,1018	1210,1140,1020
	Pyrrole ring	842, 760, 699	840,768,688
WD-PTh	OH stretching	3424	3445,3250
	C=C stretching	1523,1424,1409,1323	1524,1430,1400,1320
	C-S-C stretching	1021,1019	1130,1010
	thiophene ring	952,908,701	955,918,705
WD-PPy/PTh-4/1	OH/NH	3438	3622,3459
	C=N stretching	1566,1435,1409	1564,1430,1397
	C=C stretching	1402,1285,1021	1408,1282,1025
	C-S-C stretching	1134,1095	1138,1093
	Pyrrole /thiophene ring	952,904,744,680	950,909,777,675
WD-PPy/PTh-1/1	OH/NH	3417	3620, 3422
	C=N stretching	1566,1435,1017	1565,1432,1018
	C=C stretching	1361,1224	1371,1248
	C-S-C stretching	1142,1013	1138,1018
	Pyrrole /thiophene ring	951,754,698	958,747,710
WD-PPy/PTh-1/4	OH/NH	3415	3650,3244
	C=N stretching	1578,1435,1019	1570,1430,1015
	C=C stretching	1409,1354,1316	1408,1355,1317
	C-S-C stretching	1252	1255
	Pyrrole /thiophene ring	974,905,804,745,700	976,908,800,740,655

The IR spectrum of WD-PPy/PTh-4/1, (provided in supplementary information as Figure S3(c)) , Table 1, showed NH stretching vibration at 3438 cm^{-1} in the experimental and at 3622 cm^{-1},3459 cm^{-1} in the theoretical spectrum respectively. The C=N stretching peaks were noticed at 1566 cm^{-1},1435 cm^{-1} and 1017 cm^{-1} in the experimental spectrum and at 1564 ,1430 cm^{-1} 1397 cm^{-1} in the theoretical spectrum. The C=C stretching peak appeared at 1402 cm^{-1},1285 cm^{-1},1021 cm^{-1} and the C-S-C stretching vibrations were observed at 1408 cm^{-1},1282 cm^{-1} and 1205 cm^{-1} while the heterocyclic ring vibrations were seen at 952 cm^{-1},904 cm^{-1},744 cm^{-1},680 cm^{-1}. The theoretical spectrum was found to be in close agreement with the experimental spectrum. The IR spectrum of WD-PPy/PTh-1/1, (provided in supplementary information as Figure S3(d)), Table 1, showed NH stretching vibration was noticed at 3417 cm^{-1}. The C=N stretching peaks were found at noticed at 1566 cm^{-1},1435 cm^{-1} and 1017 cm^{-1}. The C=C stretching peak appeared at 1361 cm^{-1},1224 cm^{-1} and the C-S-C stretching peaks were noticed at 1142 cm^{-1}, 1013 cm^{-1}. The heterocyclic ring vibrations were observed at 951, cm^{-1}, 754 cm^{-1}, and 698 cm^{-1} respectively. Likewise, the IR spectrum of WD-PPy/PTh-1/4, (provided in supplementary information as Figure S3(e)), Table 1, exhibited NH stretching vibration peak at 3415 cm^{-1} and the C=N stretching vibration appeared at 1578 cm^{-1}, 1435 cm^{-1}, and 1019 cm^{-1}, while the C=C stretching peaks were found at 1409 cm^{-1},1354 cm^{-1},1316 cm^{-1}. The C-S-C stretching vibration peaks appeared at 1252 cm^{-1} . The theoretical spectrum also revealed the same peaks with a minor shift and presence of the peaks associated with WD-PPy, WD-PTh confirmed the polymerization. The experimental spectra in all cases were found to be in close agreement with the theoretical spectra.

DFT studies: Muliken charge distribution and frontier molecular orbitals.

The geometry optimized structures of WD-PPy, WD-PTh, WD-PPy/PTh-4/1, WD-PPy/PTh-1/1, and WD-PPy/PTh-1/4 are depicted in Figure 2(a-e). The geometries were optimized taking 8 units of pyrrole ring and thiophene ring for WD-PPy and WD-PTh respectively. For the co-oligomers, the ratios were taken to be 2 units of thiophene ring and 8 units of pyrrole ring for WD-PPy/PTh-4/1, 4 units of thiophene ring and 4 units of pyrrole ring for WD-PPy/PTh-1/1 and 8 units of thiophene ring and 2 units of pyrrole ring for WD-PPy/PTh-1/4. This optimization was chosen based on our DFT calculations of alternating-like, random, as well as block sequences with PPy.

(a)

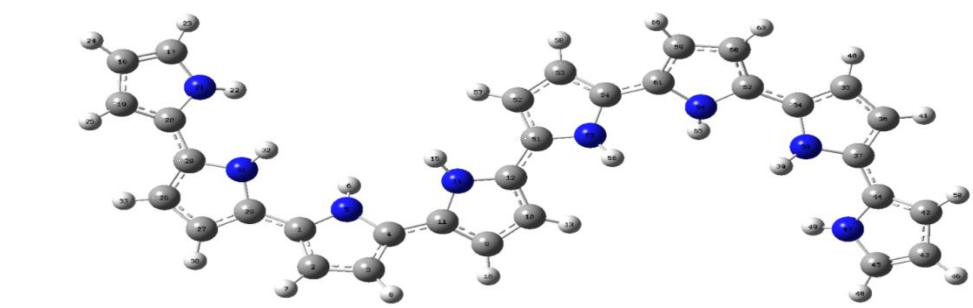

(b)

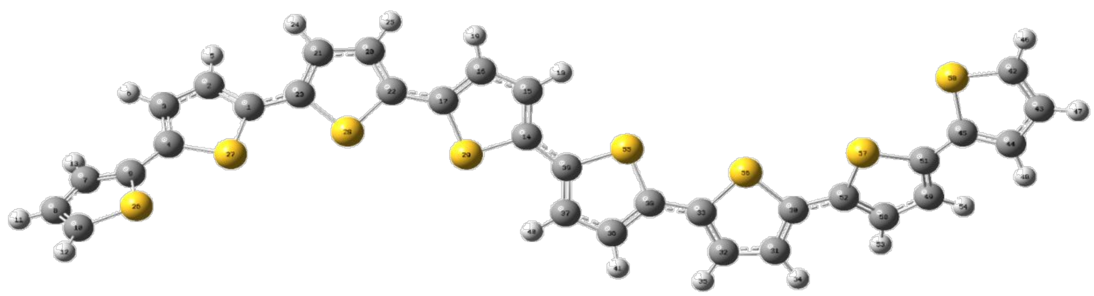

(c)

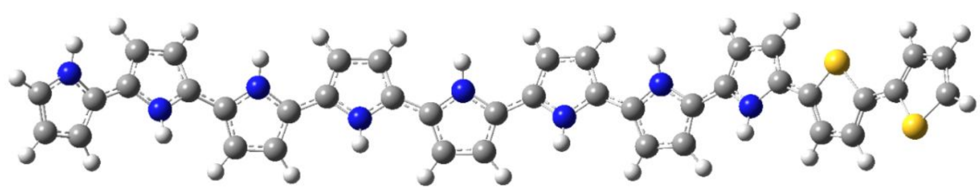

(d)

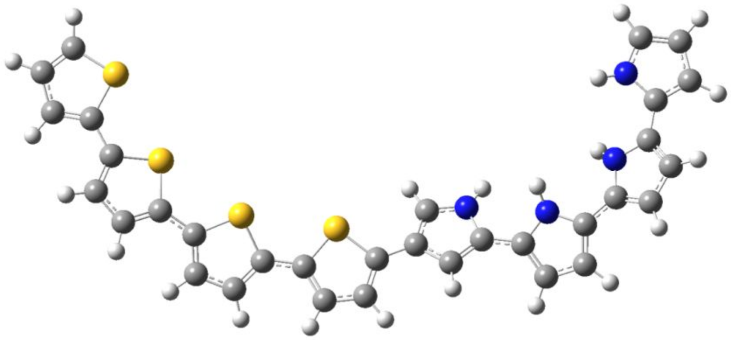

(e)

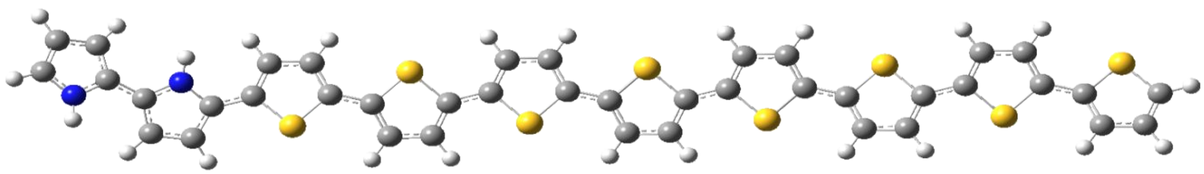

Figure 2 Optimized geometries of (a) WD-PPy,(b)WD-PTh, (c) WD-PPy/PTh-4/1, (d) WD-PPy/PTh-1/1, (e) WD-PPy/PTh-1/4

and PTh that could match with the experimental studies. Only block structures were used in the model as they were in close agreement with the experimental data. The rest of the calculations did not match with the experimental results. For WD-PPy, Figure 2(a), the C-C and C=C bond lengths were computed to be 1.42 Å and 1.39 Å. The N-H bond length was computed to be 1.007 Å and the C-N bond length was found to be 1.39 Å. Similarly, for WD-PTh, Figure 2(b), the C-C bond length was found to be 1.44 Å, the C=C bond was calculated to be 1.38 Å, while the C-S bond length was computed to be 1.75 Å. The geometry optimized structure of WD-PPy/PTh-4/1, Figure 2(c), showed C-C and C=C bond lengths to be 1.44 Å and 1.39 Å respectively while the NH bond length was computed to be 1.008 Å. The C-N and C-S bond lengths were computed to be 1.38 Å and 1.75 Å respectively. The geometry optimized structure of WD-PPy/PTh-1/1, Figure 2(d), (e) revealed the bond lengths be similar to the pervious co-oligomer. The pristine

WD-PPy and WD-PTh showed twisting of the chains but upon insertion of thiophene/pyrrole, the structures attained planar configuration, Figure 2(c), (d), (e).

Mulliken charge distribution

The charge distribution in WD-PPy, Figure 3(a) was concentrated on nitrogen atoms of pyrrole ring, and for WD-PTh, Figure 3(b), it was noticed to be concentrated over the terminal carbon atoms of the thiophene ring. For WD-PPy/PTh-4/1, WD-PPy/PTh-1/1, WD-PPy/PTh-1/4, the charge distribution was similar to the parent oligomer and did not show any significant change upon co-oligomerization.

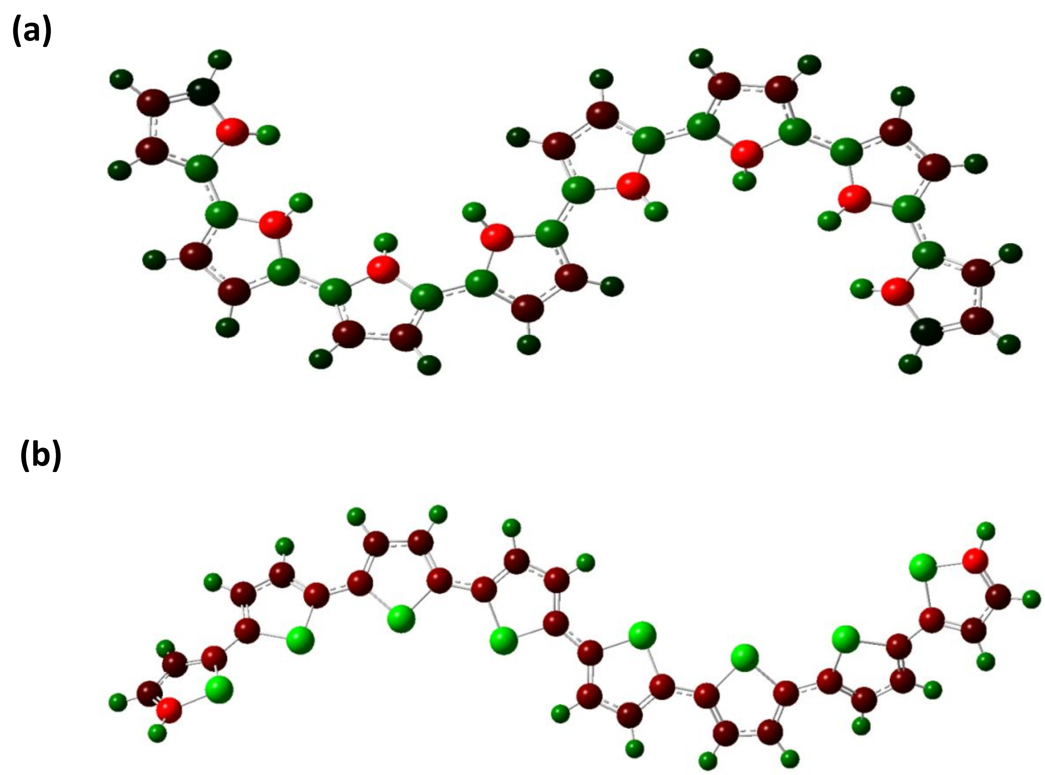

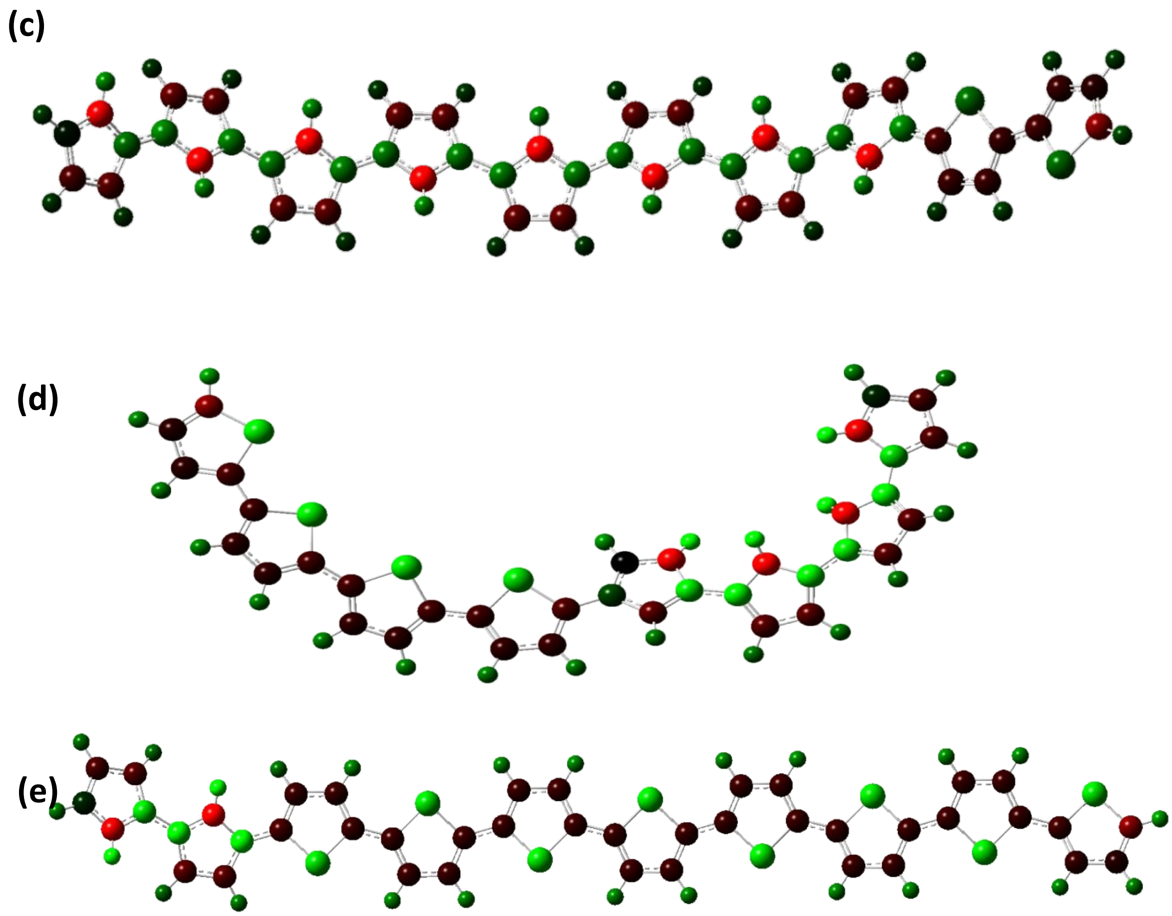

Figure 3 Muliken charge distribution in (a) WD-PPy,(b)WD-PTh, (c) WD-PPy/PTh-4/1, (d) WD-PPy/PTh-1/1, (e) WD-PPy/PTh-1/4

Molecular electrostatic potential (MEP)

The molecular electrostatic potential (MEP) is depicted in, Figure 4(a-e). For WD-PPy, Figure 4(a), the MEP is noticed to be blue around the NH bonds indicating maximum electrostatic potential. Similarly, for WD-PTh, Figure 4(b), the MEP was noticed to be in the yellow region indicating lower electrostatic potential. Interestingly, for WD-PPy/PTh-4/1, WD-PPy/PTh-1/1 and WD-PPy/PTh-1/4, Figure 4(c), (d), (e), the MEP was noticed to be intermediate of the pristine polymers. The electrostatic potential can help predict chemical reactivity as regions of negative potential are sites of protonation and nucleophilic attack, while regions of positive potential indicate electrophilic sites. In our case the co-oligomers show sites of protonation and nucleophilic attack. The highest occupied molecular orbital (HOMO) and lowest unoccupied molecular orbital (LUMO) were noticed to be uniformly delocalized in case of WD-PPy, Figure 5(a). The band gap was calculated to be 3.29 eV. The HOMO-LUMO orbitals were found to be uniformly distributed in WD-PTh as well and the band gap in this case was computed to be 2.71 eV, Figure 5(b). For WD-PPy/PTh-4/1, Figure 5(c), the band gap was computed to be 1.66 eV. The LUMO orbitals were noticed to be concentrated around the thiophene rings and the pyrrole units attached to the thiophene rings, while the HOMO orbitals were uniformly delocalized throughout the structure. Likewise, for WD-PPy/PTh-1/1, Figure 5(d), the LUMO orbitals were highly delocalized around the thiophene units and the HOMO orbitals were noticed to be concentrated around the pyrrole units. The band gap was found to be 1.72 eV which was found to be higher than the previous case. The delocalized distribution of LUMO orbitals was noticed for WD-PPy/PTh-1/4, Figure 5(e), while the HOMO orbitals were distributed over the thiophene units. The band gap was computed to be 1.56 eV.

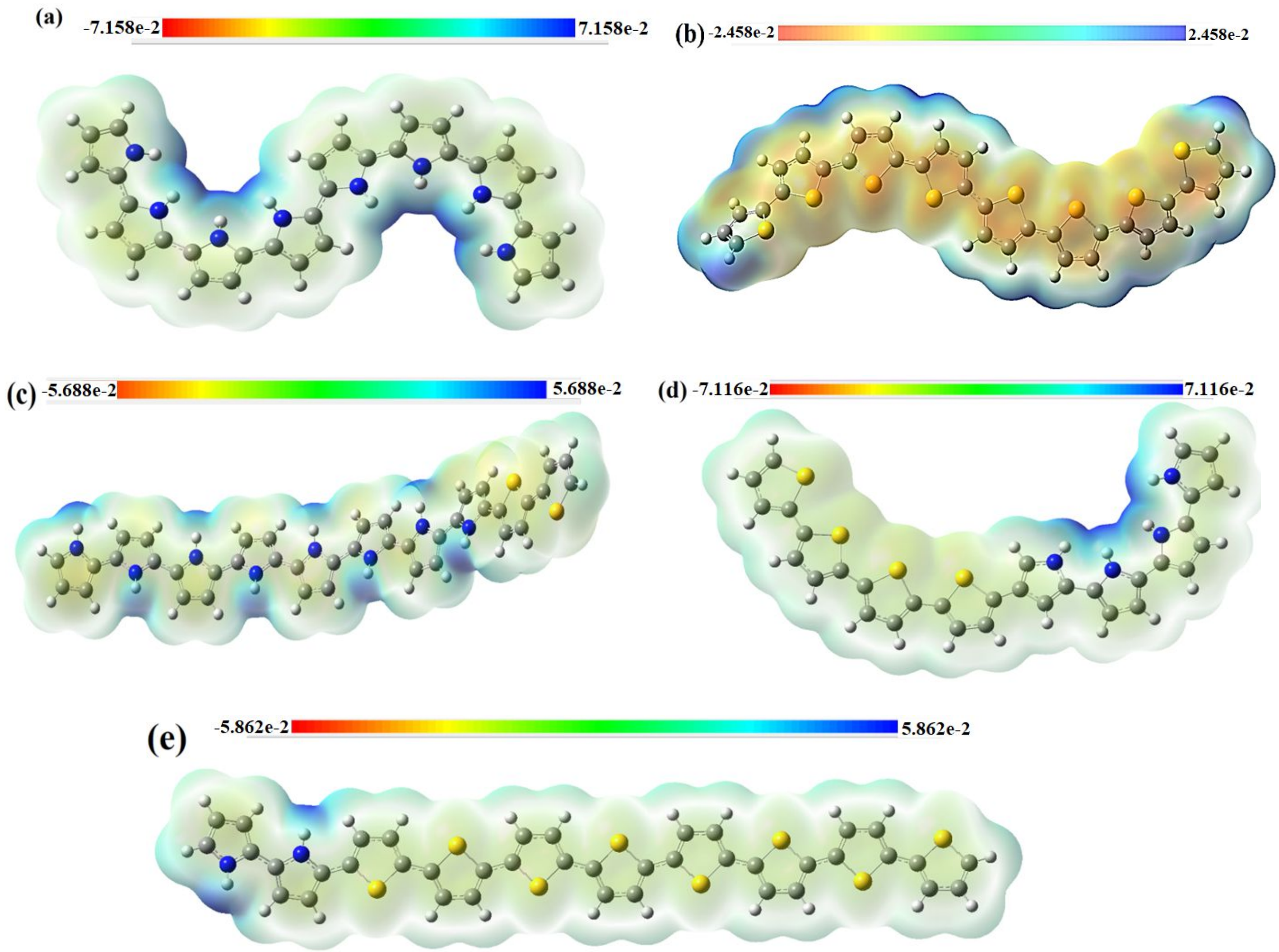

Figure 4 MEP of (a) WD-PPy, (b) WD-PTh, (c) WD-PPy/PTh-4/1, (d) WD-PPy/PTh-1/1, (e) WD-PPy/PTh-1/4

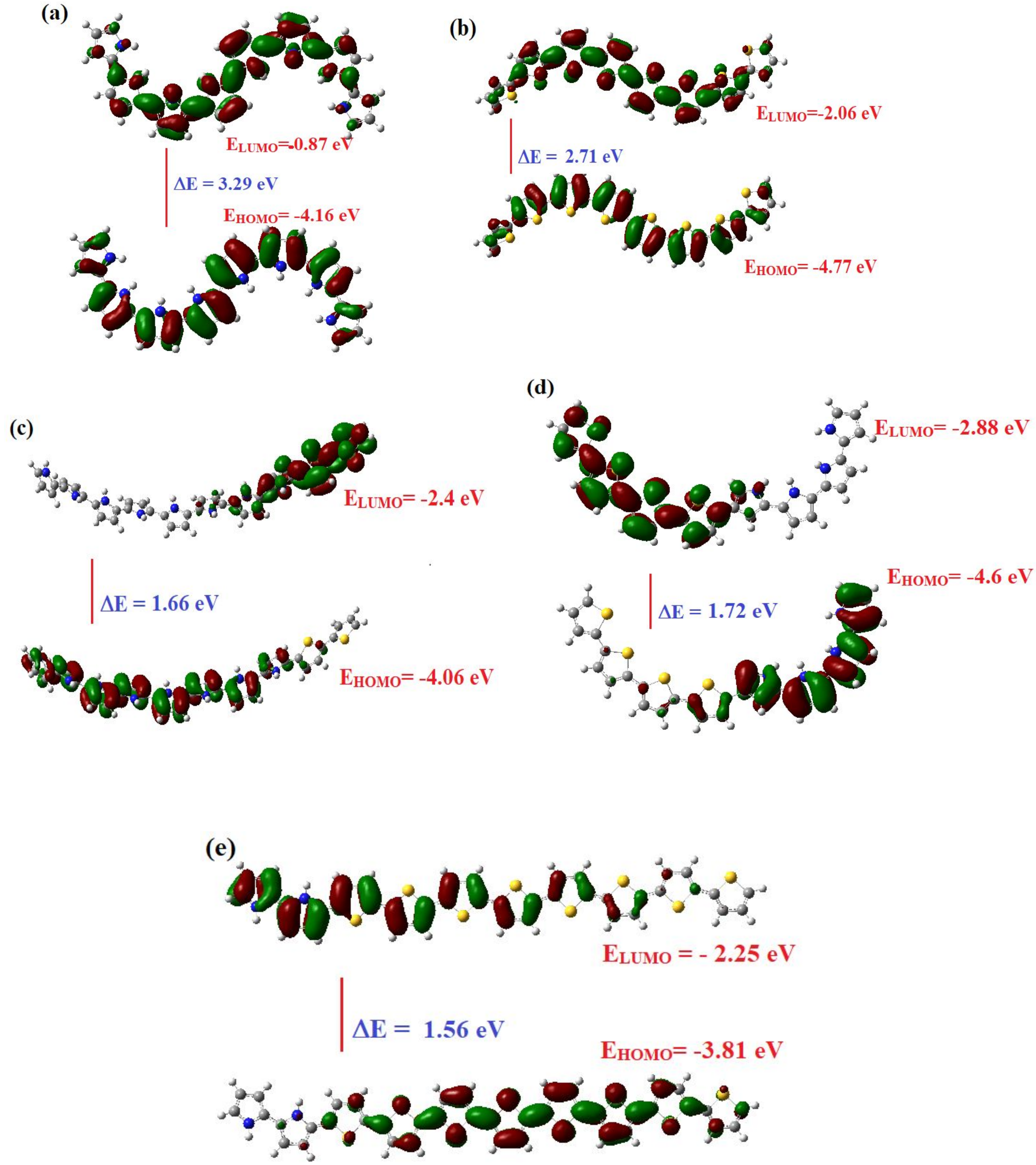

Figure 5 HOMO-LUMO distributions in (a) WD-PPy, (b) WD-PTh, (c) WD-PPy/PTh-4/1, (d) WD-PPy/PTh-1/1, (e) WD-PPy/PTh-1/4

Hence, it can be concluded that the band gap could be optimized to desirable values by the incorporation of required units of pyrrole/thiophene rings.

The UV–visible spectrum of WD-PPy, Figure 6 (a), exhibited two intense peaks at 260 nm due to the n-π* transitions and 450 nm due to π-π* transition. The theoretical spectrum (given in set) revealed the n-π* transitions at 300 nm and the π-π*transitions were noticed at 430 nm [29]. The oscillator strength of the later peak was computed to be 1.8. The UV spectrum of WD-PTh, Figure 6 (b), revealed n-π* transitions at 250nm (a shoulder), and 320 nm, while the π-π* transition peak was 450 nm [19]. The theoretical spectrum showed n-π* and π-π* transitions to be similar to the ones found in the experimental spectrum and the oscillator strength of the 450 nm peak was computed to be 1.7. The UV spectrum of WD-PPy/PTh-4/1, Figure 6 (c), exhibited intense peaks at 250 nm, 360 nm, and 440 nm and the theoretical spectrum revealed similar peaks with the oscillator strength of peak at 440 nm to be 1.4. The UV spectrum of WD-PPy/PTh-1/1, Figure 6 (d), exhibited pronounced peaks at 250 nm, 400 nm, and 600 nm and the UV-spectrum of WD-PPy/PTh-1/4, Figure 6(e) revealed an intense peak at 450 nm. The theoretical spectra showed transitions which were found to be in close agreement with the experimental spectra. The electronic transitions were found to vary with the number of pyyrole/ thiophene units in the co-oligomers and the π -π* transition were noticeably prominent for higher loading of pyrrole in WD-PPy/PTh-4/1.

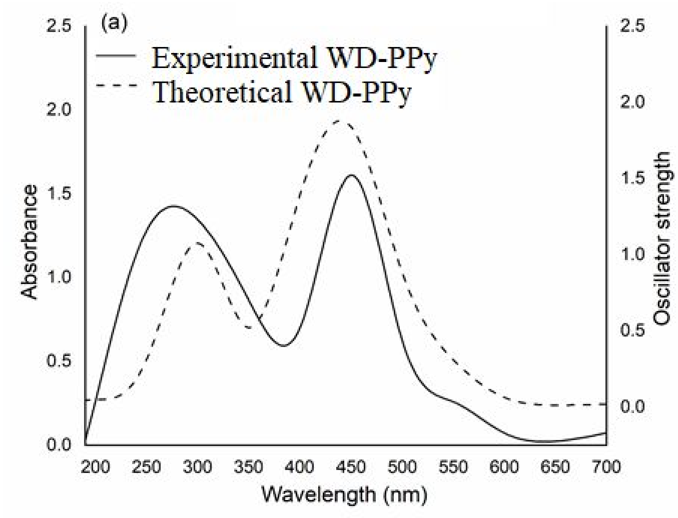
(a)
Experimental WD-PPy
Theoretical WD-PPy
Absorbance
Oscillator strength
Wavelength (nm)

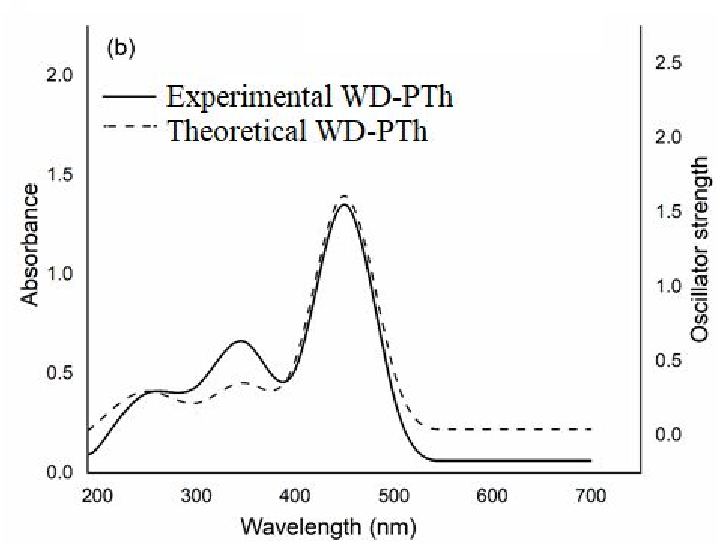
(b)
Experimental WD-PTh
Theoretical WD-PTh
Absorbance
Oscillator strength
Wavelength (nm)

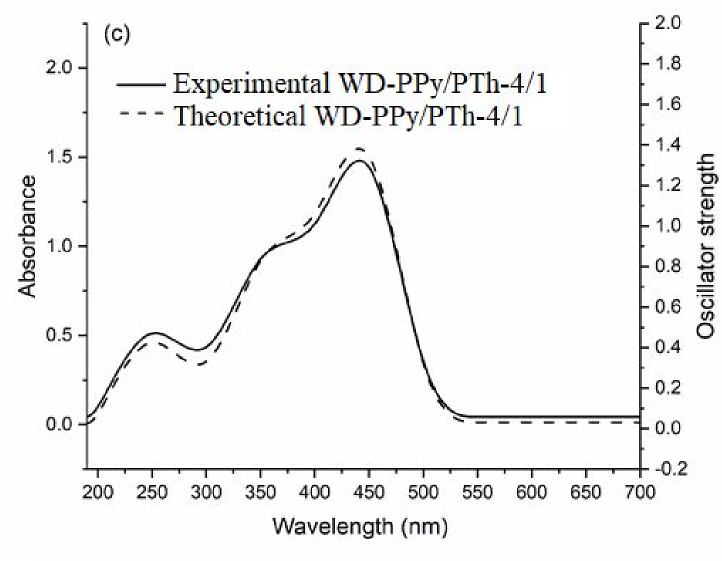
(c)
Experimental WD-PPy/PTh-4/1
Theoretical WD-PPy/PTh-4/1
Absorbance
Oscillator strength
Wavelength (nm)

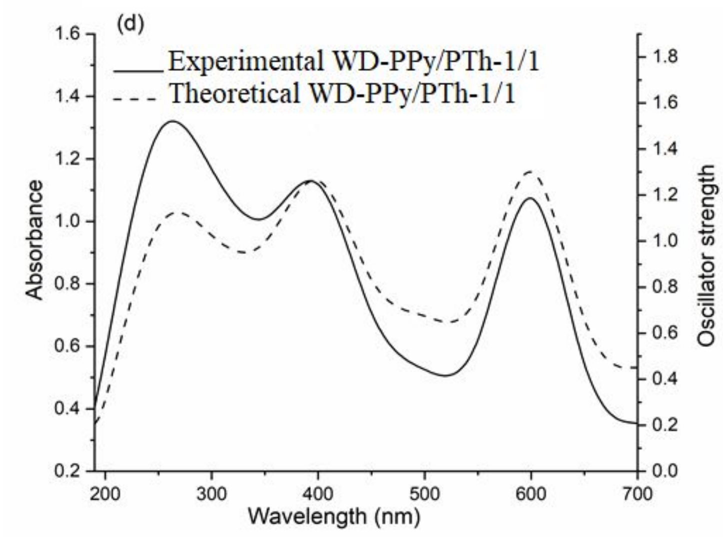
(d)
Experimental WD-PPy/PTh-1/1
Theoretical WD-PPy/PTh-1/1
Absorbance
Oscillator strength
Wavelength (nm)

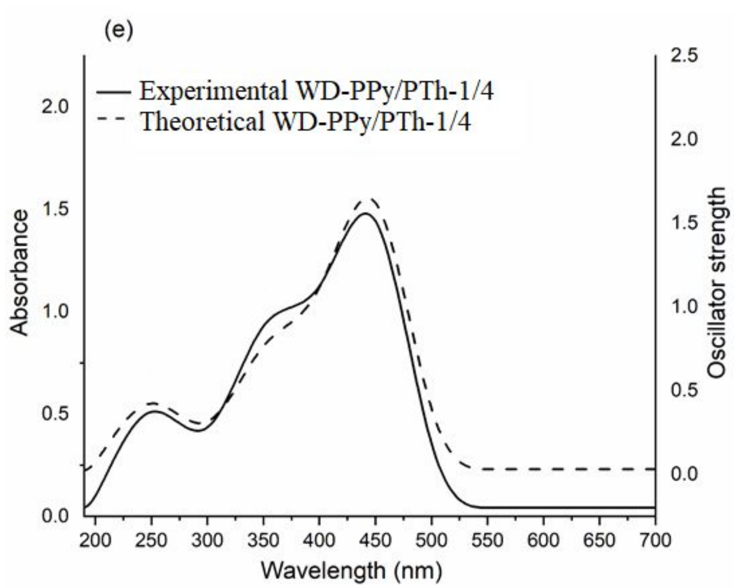

Figure 6 UV-visible spectra of (a) WD-PPy, (b) WD-PTh, (c) WD-PPy/PTh-4/1, (d) WD-PPy/PTh-1/1, (e) WD-PPy/PTh-1/4

Biophysical interaction studies

In this study, UV–vis spectra of BSA as well as HSA were taken at different concentrations of WD-PPy, WD-PTh, WD-PPy/PTh-4/1, WD-PPy/PTh-1/1, and WD-PPy/PTh-1/4 (50 uL – 300 uL for BSA and 50 uL – 500 uL for HSA) to investigate the binding of the macromolecules to the oligomers. The UV–vis absorption spectrum of BSA, Figure 7 (a), in absence of oligomer showed a prominent peak at 280 nm associated with the presence of aromatic amino acids. Likewise, the UV–vis absorption spectrum of HSA, Figure 8 (a), showed a prominent peak at 275 nm associated with the presence of aromatic amino acids.

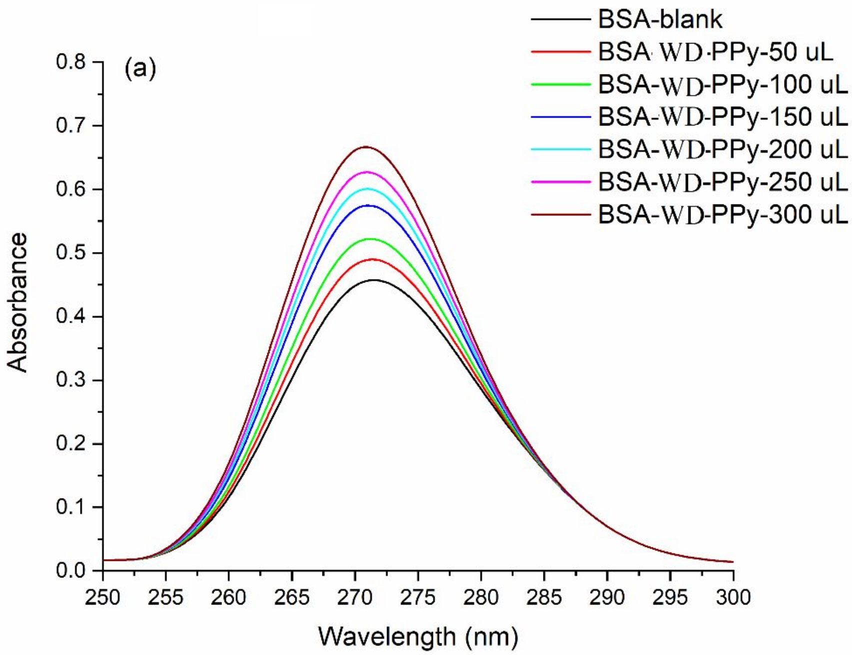
(a)
BSA-blank
BSA WD PPy-50 uL
BSA-WD-PPy-100 uL
BSA-WD-PPy-150 uL
BSA-WD-PPy-200 uL
BSA-WD-PPy-250 uL
BSA-WD-PPy-300 uL
Absorbance
Wavelength (nm)

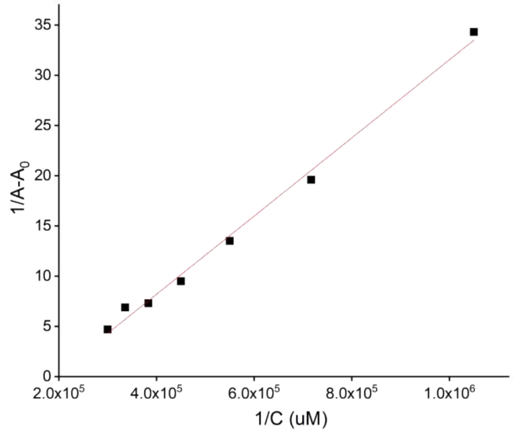
1/A-A0
1/C (uM)

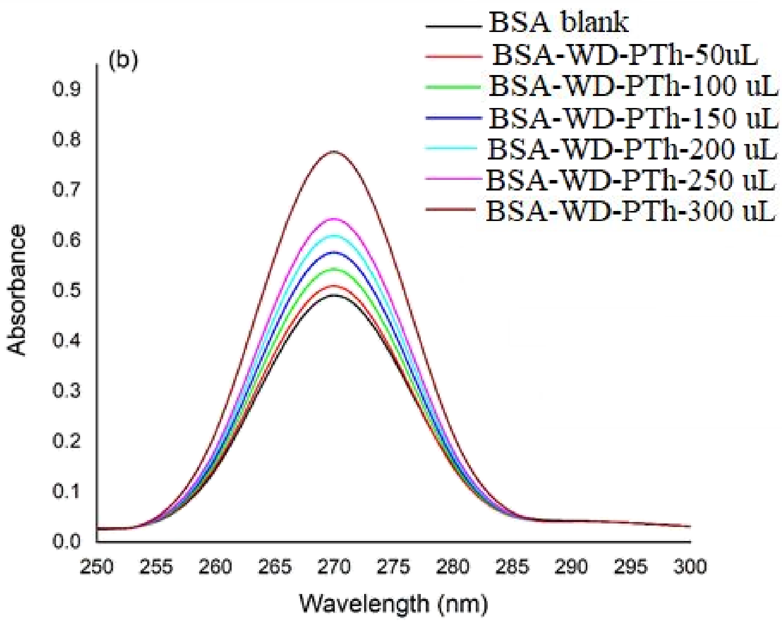
(b)
BSA blank
BSA-WD-PTh-50uL
BSA-WD-PTh-100 uL
BSA-WD-PTh-150 uL
BSA-WD-PTh-200 uL
BSA-WD-PTh-250 uL
BSA-WD-PTh-300 uL
Absorbance
Wavelength (nm)

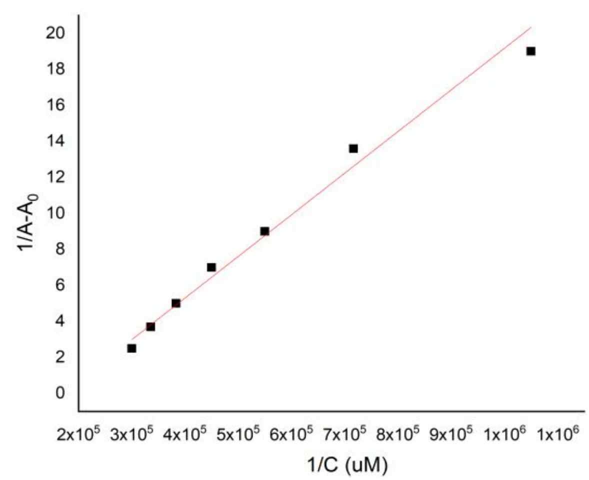
1/A-A0
1/C (uM)

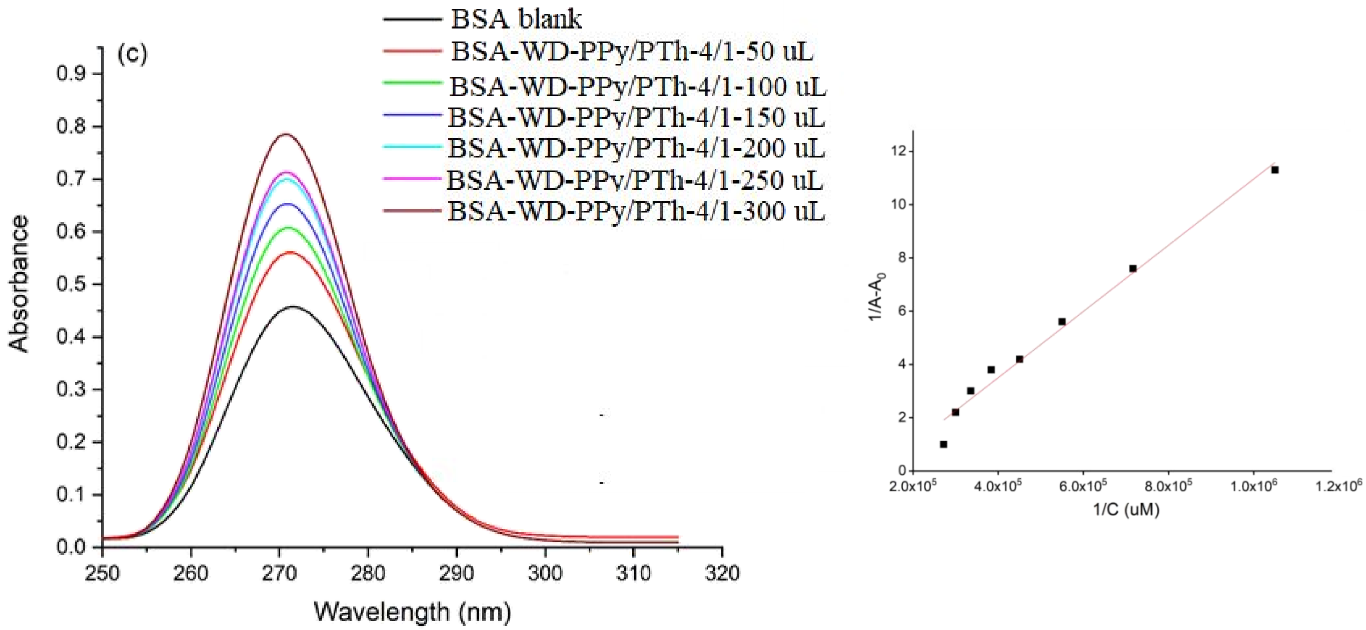
(c)
BSA blank
BSA-WD-PPy/PTh-4/1-50 uL
BSA-WD-PPy/PTh-4/1-100 uL
BSA-WD-PPy/PTh-4/1-150 uL
BSA-WD-PPy/PTh-4/1-200 uL
BSA-WD-PPy/PTh-4/1-250 uL
BSA-WD-PPy/PTh-4/1-300 uL
Absorbance
Wavelength (nm)
1/A-A0
1/C (uM)

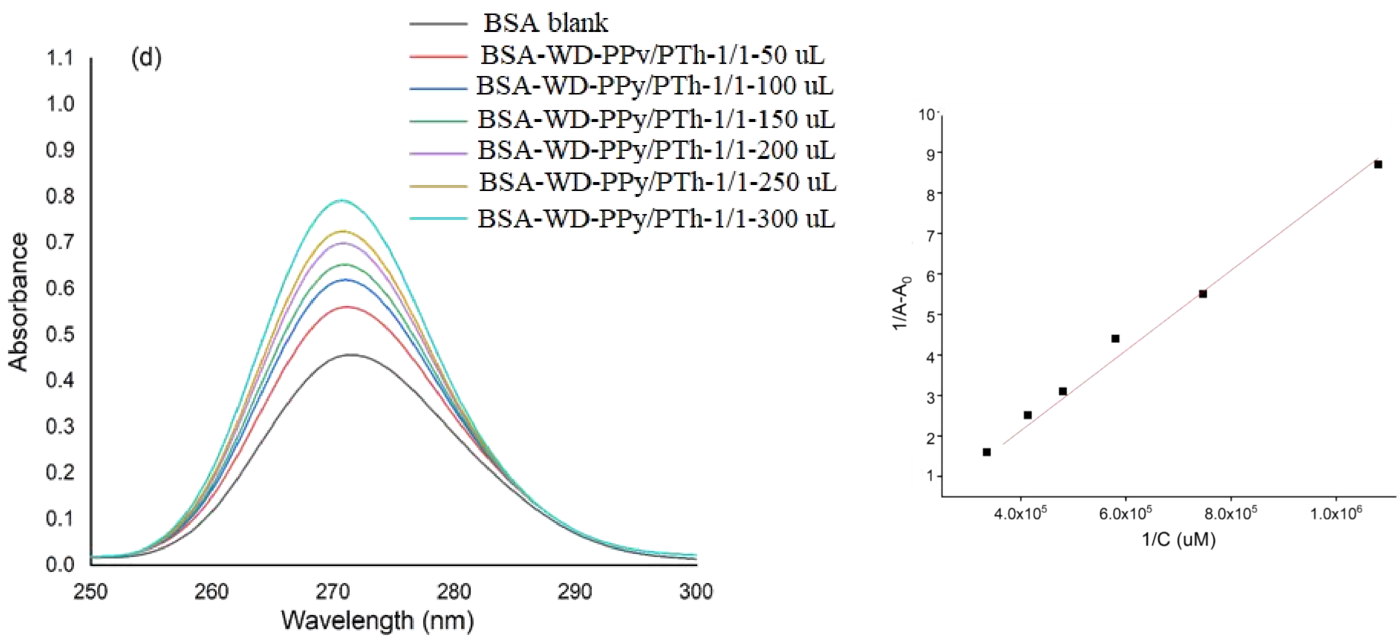
(d)
BSA blank
BSA-WD-PPy/PTh-1/1-50 uL
BSA-WD-PPy/PTh-1/1-100 uL
BSA-WD-PPy/PTh-1/1-150 uL
BSA-WD-PPy/PTh-1/1-200 uL
BSA-WD-PPy/PTh-1/1-250 uL
BSA-WD-PPy/PTh-1/1-300 uL
Absorbance
Wavelength (nm)
1/A-A0
1/C (uM)

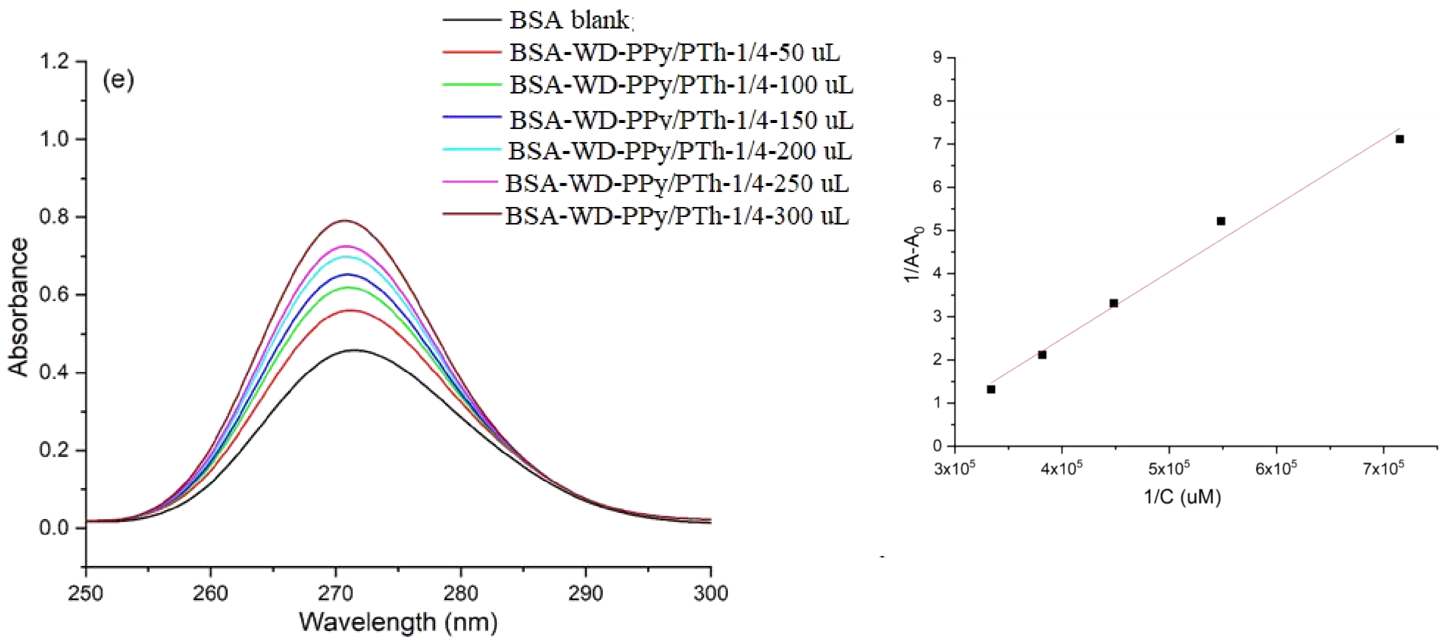

Figure 7 UV–vis absorption spectra of BSA in (a) WD-PPy, (b)WD-PTh ,(c) WD-PPy/PTh-4/1, (d) WD-PPy/PTh-1/1, (e) WD-PPy/PTh-1/4 (inset plot of $1/(A - A_0)$ vs. 1/[C])

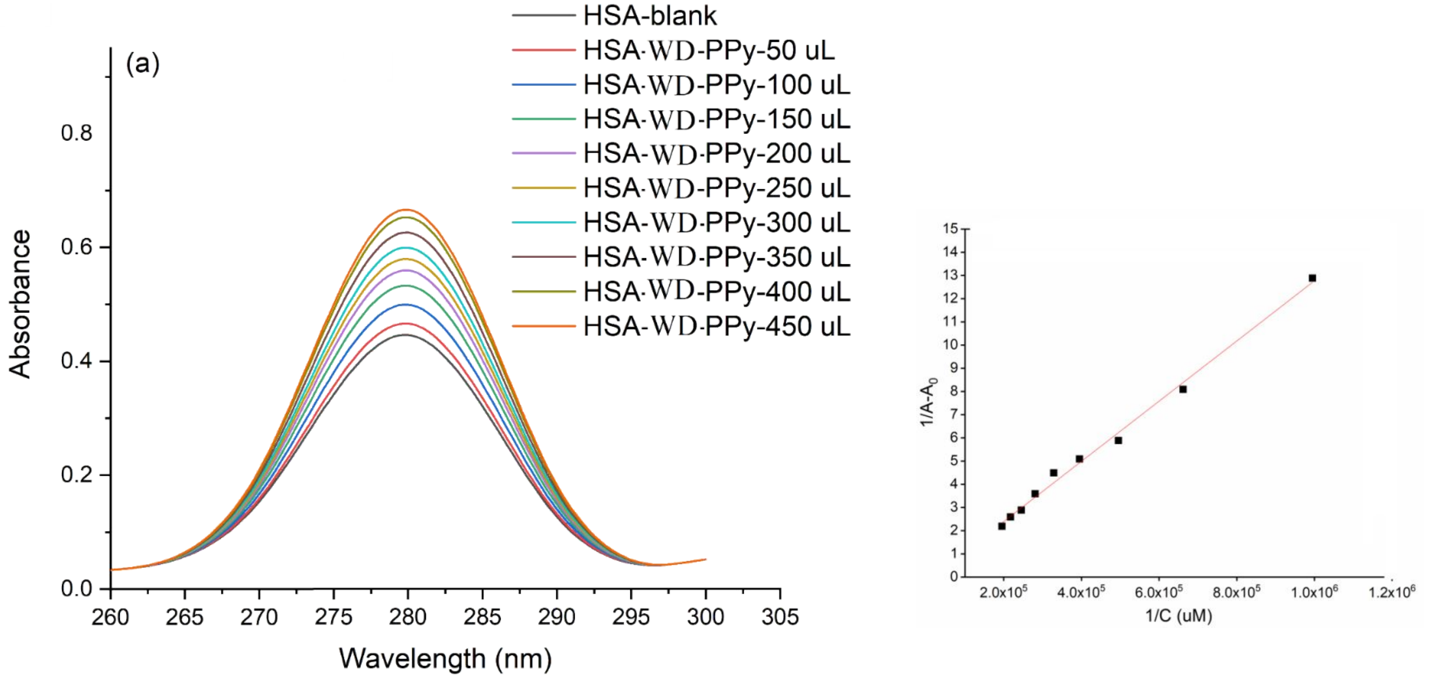
(a)
Absorbance
Wavelength (nm)
HSA-blank
HSA-WD-PPy-50 uL
HSA-WD-PPy-100 uL
HSA-WD-PPy-150 uL
HSA-WD-PPy-200 uL
HSA-WD-PPy-250 uL
HSA-WD-PPy-300 uL
HSA-WD-PPy-350 uL
HSA-WD-PPy-400 uL
HSA-WD-PPy-450 uL
0.0 0.2 0.4 0.6 0.8
260 265 270 275 280 285 290 295 300 305
$1/A-A_0$
1/C (uM)
0 1 2 3 4 5 6 7 8 9 10 11 12 13 14 15
$2.0x10^5$ $4.0x10^5$ $6.0x10^5$ $8.0x10^5$ $1.0x10^6$ $1.2x10^6$

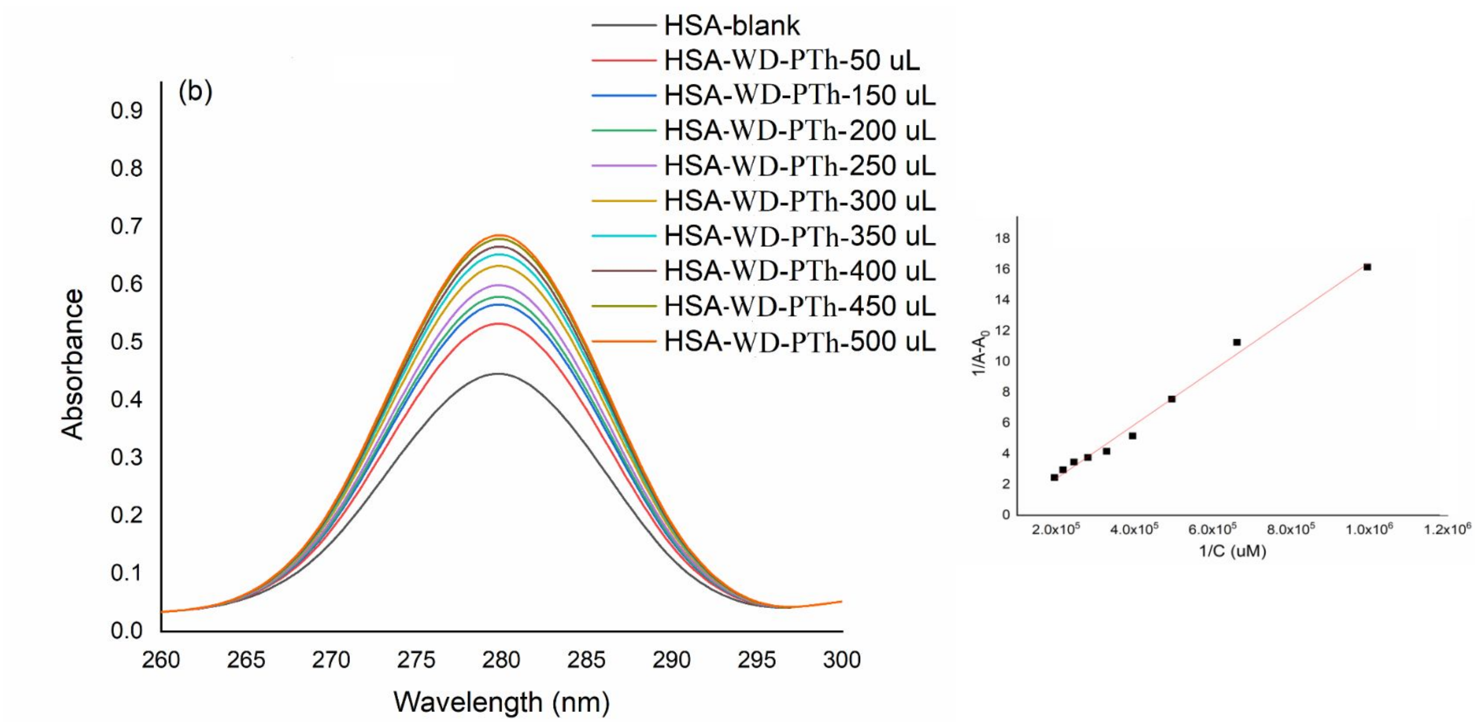
(b)
Absorbance
Wavelength (nm)
HSA-blank
HSA-WD-PTh-50 uL
HSA-WD-PTh-150 uL
HSA-WD-PTh-200 uL
HSA-WD-PTh-250 uL
HSA-WD-PTh-300 uL
HSA-WD-PTh-350 uL
HSA-WD-PTh-400 uL
HSA-WD-PTh-450 uL
HSA-WD-PTh-500 uL
0.0 0.1 0.2 0.3 0.4 0.5 0.6 0.7 0.8 0.9
260 265 270 275 280 285 290 295 300
$1/A-A_0$
1/C (uM)
0 2 4 6 8 10 12 14 16 18
$2.0x10^5$ $4.0x10^5$ $6.0x10^5$ $8.0x10^5$ $1.0x10^6$ $1.2x10^6$

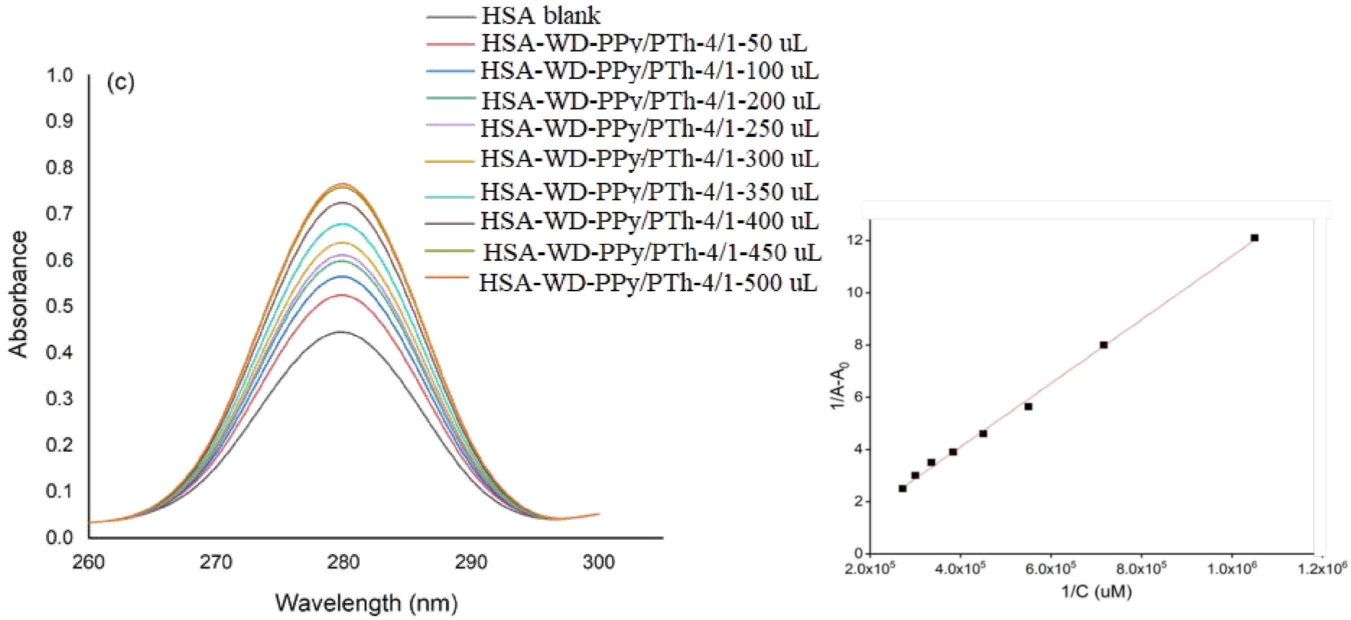
(c)
HSA blank
HSA-WD-PPy/PTh-4/1-50 uL
HSA-WD-PPy/PTh-4/1-100 uL
HSA-WD-PPy/PTh-4/1-200 uL
HSA-WD-PPy/PTh-4/1-250 uL
HSA-WD-PPy/PTh-4/1-300 uL
HSA-WD-PPy/PTh-4/1-350 uL
HSA-WD-PPy/PTh-4/1-400 uL
HSA-WD-PPy/PTh-4/1-450 uL
HSA-WD-PPy/PTh-4/1-500 uL
Absorbance
Wavelength (nm)
1/A-A0
1/C (uM)

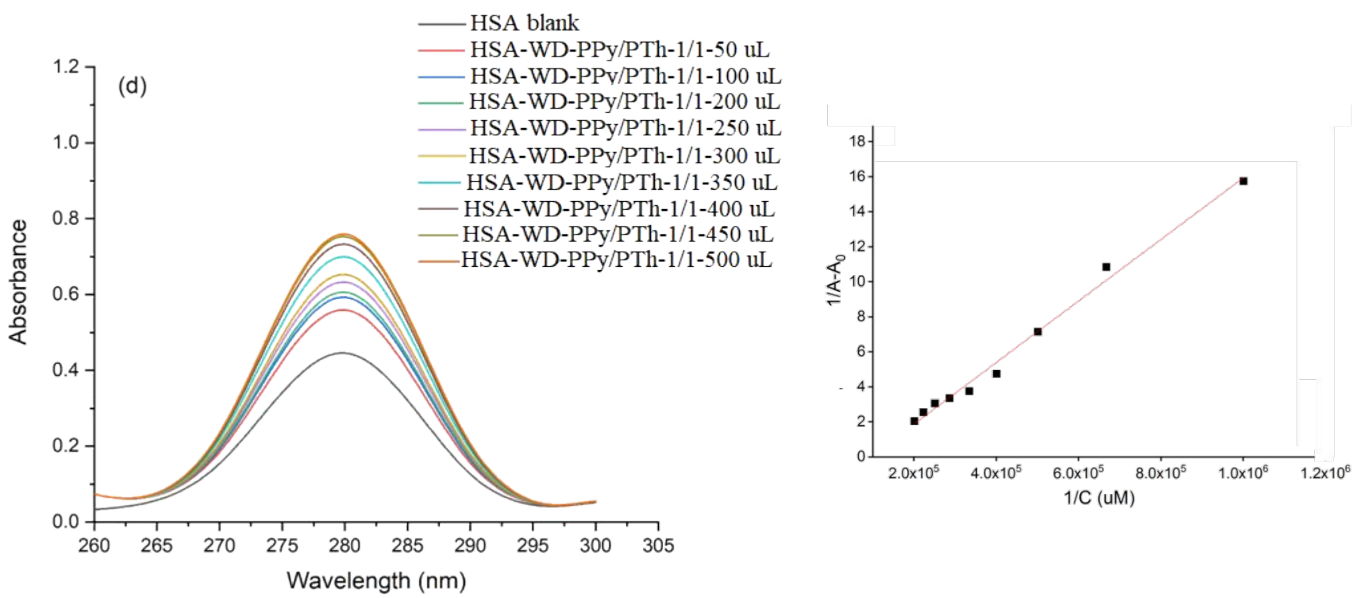
(d)
HSA blank
HSA-WD-PPy/PTh-1/1-50 uL
HSA-WD-PPy/PTh-1/1-100 uL
HSA-WD-PPy/PTh-1/1-200 uL
HSA-WD-PPy/PTh-1/1-250 uL
HSA-WD-PPy/PTh-1/1-300 uL
HSA-WD-PPy/PTh-1/1-350 uL
HSA-WD-PPy/PTh-1/1-400 uL
HSA-WD-PPy/PTh-1/1-450 uL
HSA-WD-PPy/PTh-1/1-500 uL
Absorbance
Wavelength (nm)
1/A-A0
1/C (uM)

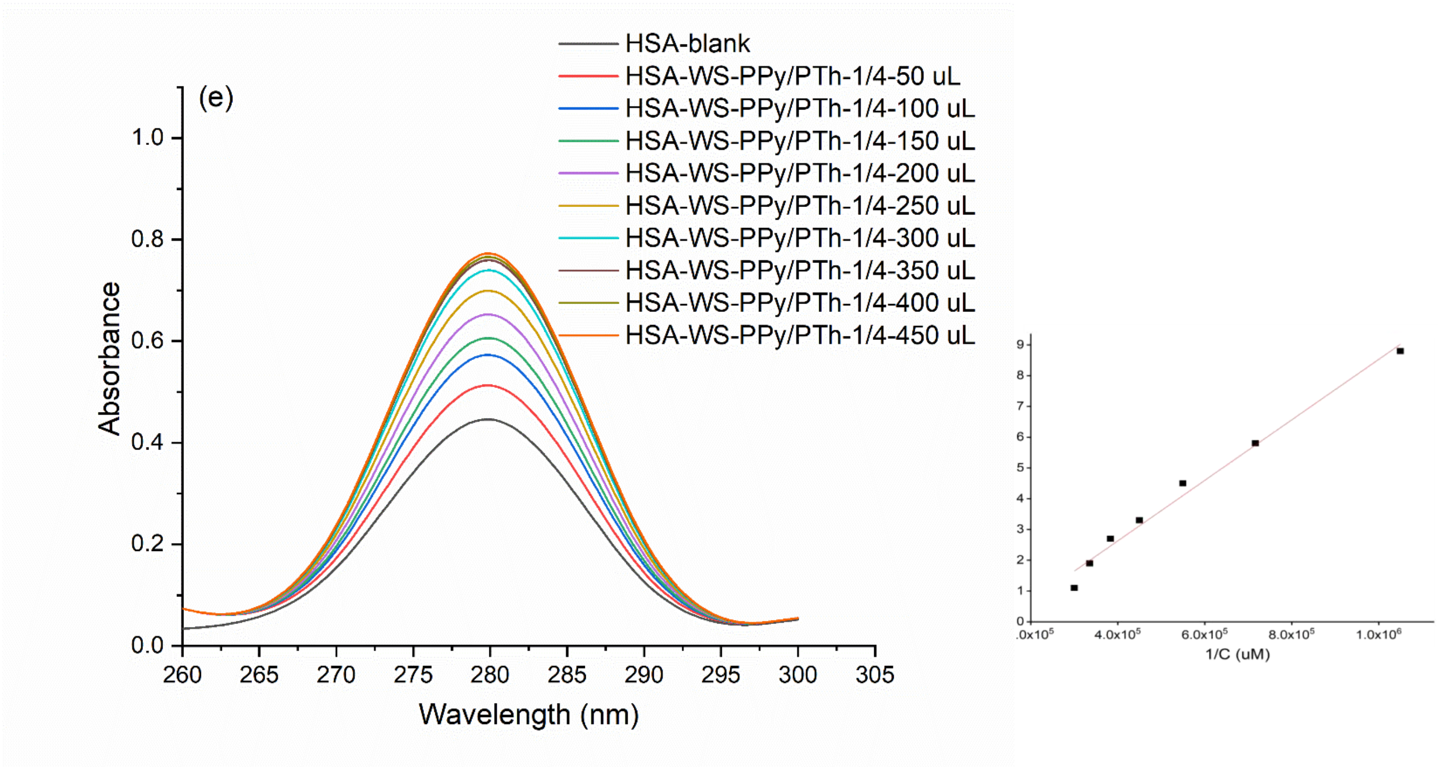

Figure 8 UV–vis absorption spectra of HSA in (a) WD-PPy, (b)WD-PTh ,(c) WD-PPy/PTh-4/1, (d) WD-PPy/PTh-1/1, (e) WD-PPy/PTh-1/4 (inset plot of $1/(A - A_0)$ vs. 1/[C])

The titration of BSA and HSA with varying concentrations of WD-PPy, Figure 7 (a), Figure 8 (a), led to the increase in absorbance thereby confirming formation of WD-PPy-BSA/HSA complex induced by binding [30-32]. The hydrophobicity of the microenvironment of the aromatic amino acid also revealed a decrease in residues be due to the losing and unfolding of the protein skeleton. The titration of BSA and HSA with varying concentrations of WD-PTh, Figure 7 (b), Figure 8 (b), also led to the increase in absorbance thereby confirming formation of WD-PPy-BSA/HSA complex induced by binding. The titration of BSA and HSA with varying concentrations of WD-PPy/PTh-4/1, WD-PPy/PTh-1/1, WD-PPy/PTh-1/4, Figure 7 (c), (d), (e), Figure 8 (c), (d),(e) showed broadening of the peak corresponding to the BSA/HSA due to higher extent of unfolding of proteins. The binding constant value (K_b) was computed by taking λ_{max} = 275 nm for BSA and 280 nm for HSA, and was found to be 2.5 × 10^4 for WD-PPy with BSA, 7.7 × 10^4 for WD-PPy with HSA. The K_b values for WD-PTh with BSA and HSA were calculated to be 4.3 × 10^4 and 5.7 × 10^4 respectively. The K_b values for WD-PPy/PTh-4/1 with BSA were found to be an order higher indicating that the co-oligomers showed a strong affinity for binding towards BSA as well as HSA, Table 2. The binding affinity was found to be higher for HSA than for BSA for all co-oligomers.

Docking studies

There are 3 types of interactions identified in the WD-PPy/PTh-4/1-BSA complex, Figure 9 (a) ,(b) Table 2. The pi-cation interaction with His18 was balanced the N atom in the polymer. The other noticeable interactions are pi-alkyl interaction with Leu 282, Lys 283, Lys 159 and pi-lone pair interaction with Lys12. The binding energy was computed to be -8.78 kcal/mol. There were 2 hydrogen bond interactions noticeable in WD-PPy/PTh-1/1-BSA complex, Figure 9 (c), (d), Table 2, with His 145 and Tyr 45. The 6 pi-pi bond interactions were found with Arg196, Arg435, Cys 447, Ile 455, Lys 431 and Pro 146 while pi-ionic interactions were noticed for Arg458, Asp 108, Glu 186, Lys 439 respectively. The binding energy was computed to be -9.88 kcal/mol. For WD-PPy/PTh-1/4-BSA complex, Figure 9 (e), (f), 5 hydrogen bond interactions were noticeable with Asp72,

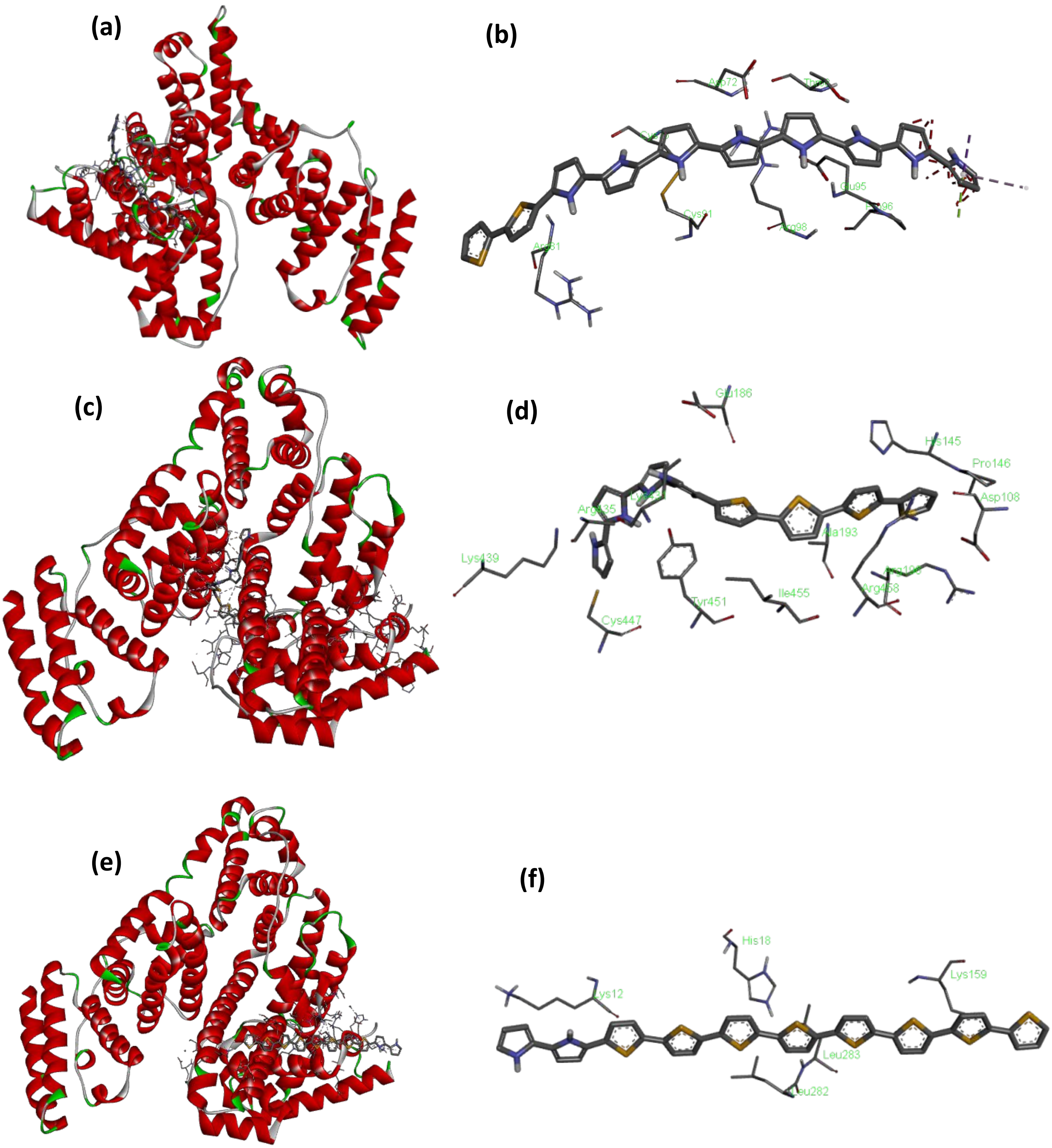

Figure 9 Binding orientations of the lowest docking energy conformations of oligomer-co-oligomer at sites I of BSA (a) WD-PPy/PTh-4/1-BSA complex, (b) amino acids residues for WD-PPy/PTh-4/1-BSA complex zoomed in within 5Å (3-D),(c) WD-PPy/PTh-1/1-BSA complex,(d) amino acids residues for WD-PPy/PTh-1/1-BSA complex zoomed in within 5Å (3-D),(e) WD-PPy/PTh-1/4-BSA complex (f) amino acids residues for WD-PPy/PTh-1/4-BSA complex zoomed in within 5Å (3-D)

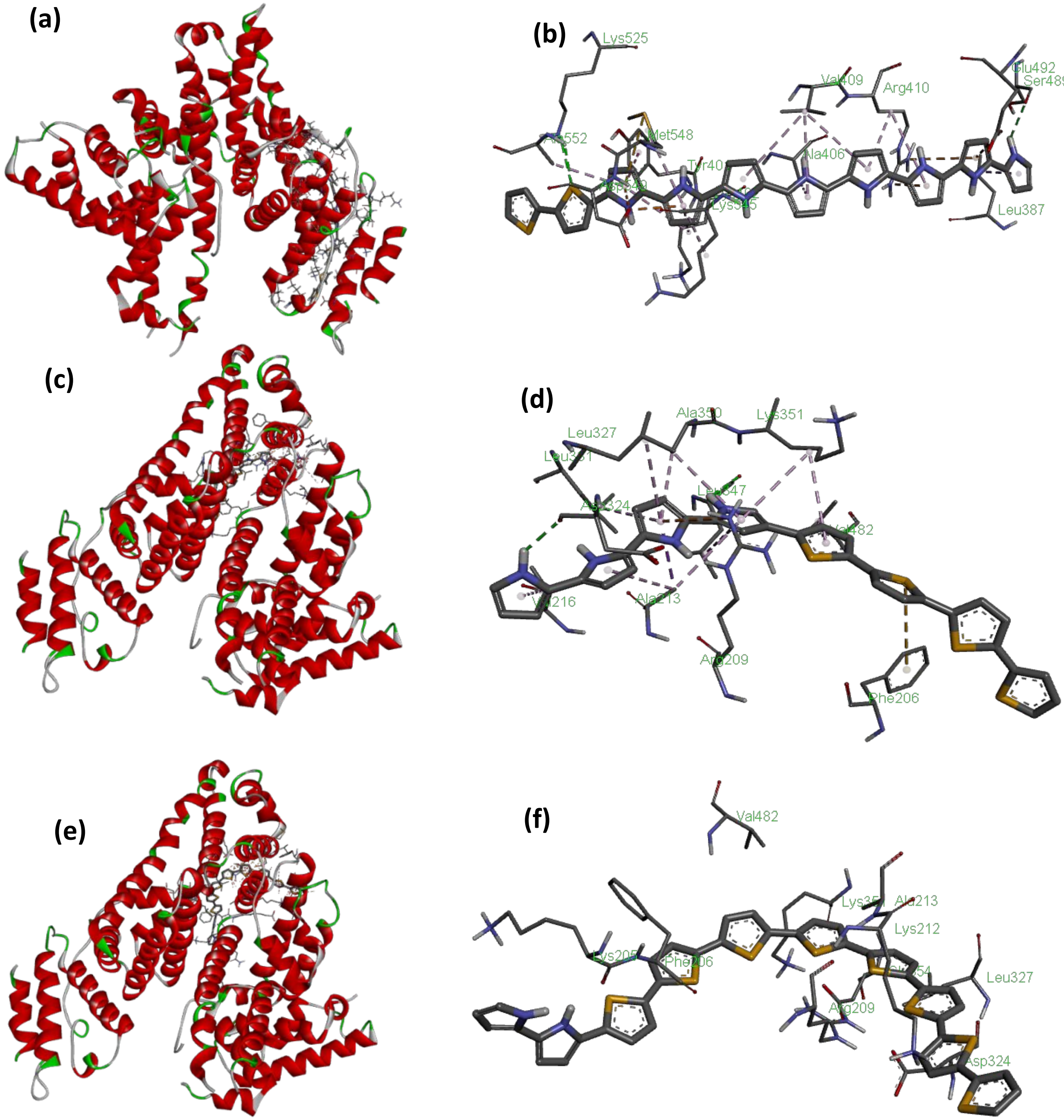

Figure 10 Binding orientations of the lowest docking energy conformations of oligomer-co-oligomer at sites I of HSA (a) WD-PPy/PTh-4/1-HSA complex, (b) amino acids residues for WD-PPy/PTh-4/1-HSA complex zoomed in within 5Å (3-D),(c) WD-PPy/PTh-1/1-HSA complex,(d) amino acids residues for WD-PPy/PTh-1/1-HSA complex zoomed in within 5Å (3-D),(e) WD-PPy/PTh-1/4-HSA complex (f) amino acids residues for WD-PPy/PTh-1/4-HSA complex zoomed in within 5Å (3-D)

Cys 75, Cys 91, Glu 95 and Thr 68, while 2 pi-ionic interactions were present at Arg 81 and Arg98. The binding energy was computed to be -8.34 kcal/mol. The docked result of HSA complexes with WD-PPy/PTh are depicted in Figure 10 (a-e), Table 2. The WD-PPy/PTh-4/1-HSA complex, Figure10 (a), (b) revealed 7 pi-sigma interactions with Ala 213, Ala 350, Leu 327, Leu 331, Lys 351, Phe206 and Val 482 amino acids. Hydrogen bond interactions were prominent for Arg209 and Asp324, while pi-ionic interactions were notable for Glu 354, Table 2. The docked results for WD-PPy/PTh-1/1-HSA complex, Figure10 (c), (d) showed 5 pi-alkyl interactions with Ala 350, Leu 327, Leu 331, Lys 351, Val 216 and Val 482, while one pi-sigma interaction was found at Ala 213. There were 2 hydrogen bond interactions present at Asp 324 and Leu 347 and one pi-ionic interaction at Arg209. Similarly, WD-PPy/PTh-1/4-HSA complex, Figure 10 (e), (f), revealed 5 pi-alkyl interactions at Ala406, Ala552, Leu387, Lys402 and Lys545 whereas Arg 410, Asp 549, Glu 492 showed pi-ionic interactions. The amino acids Lys525 and Ser489 exhibited hydrogen bond interactions, while Lys538, Val 409 and Met548 showed pi-sigma interactions. The molecular docking results confirmed that the hydrophobic interactions and the hydrogen bonding had significant contributions to the binding energies, and pi-interactions contributed to the stabilization of the binding structures.

Table 2 Estimated binding constant (K_b) obtained using Benesi-Hildebrand equation and binding energies obtained from docking results for WD-PPy/PTh-4/1, WD-PPy/PTh-1/1 and WD-PPy/PTh-1/4

Complexes	K_b (Benesi-Hildebrand equation) (μM^{-1})	Binding Energy(kcal /mol)	List of amino acids involved in binding	Type of interactions	Distance (Å)
BSA interaction					
WD-PPy/PTh-4/1-BSA	5.2×10^5	-8.78	His18	pi-cation	3.25
			Lys12	pi-lone pair	2.89
			Leu282	pi-alkyl	5.12
			Lys283	pi-alkyl	4.94
			Lys159	pi-alkyl	4.62
WD-PPy/PTh-1/1-BSA	7.4×10^5	-9.88	Ala193	pi-sigma	3.83
			Arg196	pi-pi	4.90
			Arg435	pi-pi	4.75
			Arg458	pi-ionic	3.86
			Asp108	pi-ionic	3.68
			Cys447	pi-pi	5.27
			Glu186	pi-ionic	4.77
			His145	hydrogen bond	3.87
			Ile455	pi-pi	5.33
			Lys431	pi-pi	5.41
			Lys439	pi-ionic	3.90
			Pro146	pi-pi	4.99
			Tyr451	hydrogen bond	2.49
WD-PPy/PTh-1/4-BSA	4.6×10^5	-8.34	Arg81	pi-ionic	4.62
			Arg98	pi-ionic	4.36
			Asp72	hydrogen bond	2.27
			Cys75	hydrogen bond	2.28
			Cys91	hydrogen bond	4.50
			Glu95	hydrogen bond	2.73
			Pro96	pi-alkyl	5.06
			Thr68	hydrogen bond	2.41
HSA interaction					
WD-PPy/PTh-4/1-HSA	8.3×10^5	-8.55	Ala213	pi-sigma	3.72
			Ala350	pi-sigma	4.97
			Arg209	hydrogen bond	3.06

			Asp324	hydrogen bond	2.61
			Glu354	pi-ionic	4.81
			Leu327	pi-sigma	5.21
			Leu331	pi-sigma	5..44
			Lys205	pi-ionic	3.70
			Lys351	pi-sigma	4.43
			Phe206	pi-sigma	3.94
			Val482	pi-sigma	4.68
WD-PPy/PTh-1/1-HSA	5.4×10^5	-8.25	Ala213	Pi-sigma	4.54
			Ala350	pi-alkyl	4.89
			Arg209	pi-ionic	4.86
			Asp324	hydrogen bond	2.48
			Leu327	pi-alkyl	4.65
			Leu331	pi-alkyl	5.13
			Leu347	hydrogen bond	5.38
			Lys351	pi-alkyl	4.52
			Phe206	pi-ionic	5.32
			Val216	pi-alkyl	4.98
			Val482	pi-alkyl	4.85
WD-PPy/PTh-1/4-HSA	5.7×10^5	-8.48	Ala406	pi-alkyl	4.03
			Ala552	pi-alkyl	4.74
			Arg410	pi-ionic	4.81
			Asp549	pi-ionic	3.74
			Glu492	pi-ionic	4.44
			Leu387	pi-alkyl	3.86
			Lys402	pi-alkyl	4.51
			Lys525	hydrogen bond	4.89
			Lys538	pi-sigma	4.90
			Lys545	pi-alkyl	5.25
			Met548	pi-sigma	4.89
			Ser489	hydrogen bond	2.87
			Tyr401	pi-pi	4.91
			Val 409	pi-sigma	5.22

Conclusion

Water dispersible PPy, PTh and their co-oligomers were successfully synthesized. SEM studies confirmed the predominance of the morphology having higher loading of PPy/PTh based on its loading. ^{13}C-NMR also confirmed co-oligomerization and formation of block copolymer as shown by the experimental and theoretical FTIR studies. The theoretical as well as experimental UV studies confirmed that the electronic transitions were found to vary with the pyrrole/thiophene content in the co-oligomers. The UV studies showed increase in the intensities of BSA/HSA upon addition of PPy/PTh oligomers. The binding constant (K_b) value was computed to be 2.5×10^4 for WD-PPy with BSA, 7.7×10^4 for WD-PPy with HSA, 4.3×10^4 for WD-PTh with BSA and 5.7×10^4 for WD-PTh with HSA respectively. The K_b values were found to be higher for HSA than for BSA for all the co-oligomers. Binding energy was calculated be highest for WD-PPy/PTh-1/1-BSA complex which was -9.88 kcal/mol and -8.55 J/mol for WD-PPy/PTh-4/1-HSA. The structural understanding, binding modes are vital factors affecting the binding free energies provided valuable insights which could be utilized for designing of biosensors. The fluorescence studies of these oligomers are underway in our laboratory and will be published soon.

ASSOCIATED CONTENT

Acknowledgement

The work was funded by the National Science Foundation (Award # 2122044), the NSF PREM for Hybrid Nanoscale Systems. The corresponding authors wishes to acknowledge NSF PREM for providing financial support.

Supporting Information

^{1}H-NMR,^{13}C-NMR and IR spectra of PPy/PTh and their co-oligomers, solubility data of oligomers and co-oligomers.

Author Contributions

The manuscript was written with the contributions of all authors. All authors have given approval to the final version of the manuscript. Ufana Riaz conceptualized the work and analyzed the results while Aaliyah Farooq carried out the synthesis of oligomers, Nuzhat Mir carried out the docking studies, Faith Nwanze carried out the protein interaction studies and Fei Yang helped with the interpretation of the protein interaction studies.

Conflict of Interest

The authors declare no conflict of interest.

References

[1] Riaz, U.; Singh, N.; Banoo, S. Theoretical Studies of Conducting Polymers: A Mini Review. New J. Chem. 2022, 46, 11, 4954–4973.

[2] Diana Tzankova, Stanislava Vladimirova, Lily Peikova, M. G. Synthesis of Pyrrole and Substituted Pyrroles. J. Chem. Technol. Met. 2018, 3, 53, 451–463.

[3] Zia, J.; Fatima, F.; Riaz, U. A Comprehensive Review on the Photocatalytic Activity of Polythiophene-Based Nanocomposites against Degradation of Organic Pollutants. Catal. Sci. Technol. 2021, 11, 20, 6630–6648.

[4] Jadoun, S.; Biswal, L.; Riaz, U. Tuning the Optical Properties of Poly(o-Phenylenediamine-Co-Pyrrole) via Template Mediated Copolymerization. Des. Monomers Polym. 2018, 21, 1, 75–81.

[5] Jadoun, S.; Verma, A.; Ashraf, S. M.; Riaz, U. A Short Review on the Synthesis, Characterization, and Application Studies of Poly(1-Naphthylamine): A Seldom Explored Polyaniline Derivative. Colloid Polym. Sci. 2017, 295, 9, 1443–1453.

[6] Gupta, B.; Prakash, R. Interfacial Polymerization of Carbazole: Morphology Controlled Synthesis. Synth. Met. 2010, 160, 5, 523–528.

[7] Mohankumar, P.; Ajayan, J.; Mohanraj, T.; Yasodharan, R. Recent Developments in Biosensors for Healthcare and Biomedical Applications: A Review. Measurement 2021,167, 108293.

[8] Naskar, P.; Maiti, A.; Chakraborty, P.; Kundu, D.; Biswas, B.; Banerjee, A. Chemical Supercapacitors: A Review Focusing on Metallic Compounds and Conducting Polymers. J. Mater. Chem. A 2021, 9, 4, 1970–2017.

[9] Gao, J.; Wang, C.; Han, D.-W.; Shin, D.-M. Single-Ion Conducting Polymer Electrolytes as a Key Jigsaw Piece for next-Generation Battery Applications. Chem. Sci. 2021, 12, 40,13248–13272.

[10] Zia, J.; Riaz, U. Photocatalytic Degradation of Water Pollutants Using Conducting Polymer-Based Nanohybrids: A Review on Recent Trends and Future Prospects. J. Mol. Liq. 2021, 340, 117162.

[11] Agrahari, R.; Bayar, B.; Abubackar, H. N.; Giri, B. S.; Rene, E. R.; Rani, R. Advances in the Development of Electrode Materials for Improving the Reactor Kinetics in Microbial Fuel Cells. Chemosphere 2022, 290, 133184.

[12] Tari, K.; Khamoushian, S.; Madrakian, T.; Afkhami, A.; Łos, M. J.; Ghoorchian, A.; Samarghandi, M. R.; Ghavami, S. Controlled Transdermal Iontophoresis of Insulin from Water-Soluble Polypyrrole Nanoparticles: An In Vitro Study. Int. J. Mol. Sci. 2021, 22,22, 12479.

[13] Haldar, U.; Mondal, S.; Hazra, S.; Guin, S.; Yeasmin, L.; Chatterjee, D. P.; Nandi, A. K.Tailor Made Synthesis of Water-Soluble Polythiophene-Graft-Poly(Caprolactone-Block-Dimethyl amino ethyl Methacrylate) Copolymer and Their PH Tunable Self-Assembly and Optoelectronic Properties. Eur. Polym. J. 2022, 168, 111124.

[14] Stejskal, J.; Bober, P. Progress in Research and Applications of Conducting Polymers: Topical Issue. Chem. Pap. 2021, 75, 10, 4979–4980.

[15] Bánhegyi, G. Introduction. In Conducting Polymers for Advanced Energy Applications, CRC Press: Boca Raton, 2021; 1–27.

[16] Masuda, H.; Kaeriyanma, K. Electrochemical Polymerization of Pyrrole with Water-Soluble Polymeric Electrolyte. Synth. Met. 1995, 69, 1–3, 513–514.

[17] Lu, Y.; Shi, G.; Li, C.; Liang, Y. Thin Polypyrrole Films Prepared by Chemical Oxidative Polymerization. J. Appl. Polym. Sci. 1998, 70, 11, 2169–2172.

[18] Patil, A. O.; Ikenoue, Y.; Wudl, F.; Heeger, A. J. Water Soluble Conducting Polymers. J. Am. Chem. Soc. 1987, 109, 6, 1858–1859.

[19] Wang, F.; Li, M.; Wang, B.; Zhang, J.; Cheng, Y.; Liu, L.; Lv, F.; Wang, S. Synthesis and Characterization of Water-Soluble Polythiophene Derivatives for Cell Imaging. Sci. Rep. 2015, 5, 1, 7617.

[20] Tolani, S. B.; Craig, M.; DeLong, R. K.; Ghosh, K.; Wanekaya, A. K. Towards Biosensors Based on Conducting Polymer Nanowires. Anal. Bioanal. Chem. 2009, 393, 4, 1225–1231.

[21] Xing, S.; Zheng H., Preparation of polyaniline nanofibers using the organic solution of aniline as seed, http://www.e-polymers.org, ISSN 1618-7229.

[22] Li, X-G.; Li, J.; Meng Q-K.; Huang, M-R. Interfacial Synthesis and Widely Controllable Conductivity of Polythiophene Microparticles, J. Phys. Chem. B, 2009, 113, 9718–9727.

[23] Singh, N.; Ali, R.; Ashraf, S. M.; Rub, A.; Riaz, U. Experimental and Computational Studies of Novel Sudan-I Dye Modified Conjugated Oligomers: Efficient $^1O_2$ Generation and Antileishmanial Characteristics. Mater. Sci. Eng. B 2021, 265, 114993.

[24] Riaz, U.; Ashraf, S. M.; Jadoun, S.; Budhiraja, V.; Kumar, P. Spectroscopic and Biophysical Interaction Studies of Water-soluble Dye modified poly(o-phenylenediamine) for its Potential Application in BSA Detection and Bioimaging, Scientific Reports,2019, 9, 8544.

[25] Das, A.; Kumar, G. S. Binding Studies of Aristololactam-β-D-Glucoside and Daunomycin to Human Serum Albumin. RSC Adv. 2014, 4, 62, 33082–33090.

[26] Yasmeen, S.; Riyazuddeen. Exploring Thermodynamic Parameters and the Binding Energetic of Berberine Chloride to Bovine Serum Albumin (BSA): Spectroscopy, Isothermal Titration Calorimetry and Molecular Docking Techniques. Thermochim. Acta 2017, 655, 76–86.

[27] Maruthapandi, M.; Nagvenkar, A.P.; Perelshtein, I.; Gedanken, A. Carbon-Dot Initiated Synthesis of Polypyrrole and Polypyrrole@CuO Micro/Nanoparticles with Enhanced Antibacterial Activity. ACS Appl. Polym. Mater. 2019, 1, 5, 1181–1186.

[28] Martinez, F.; Neculqueo, G.; Veas, M.E. Synthesis of 3,3’’’-dioctyltetrathiophene oligomer, Bol. Soc. Chil. Quím, Concepción Mar, 2000, 45,1.

[29] Phukan, P.; Chetia, R.; Boruah, R.; Konwer, S.; Sarma, D. Fabrication of Polypyrrole/Cu(ii) Nanocomposite through Liquid/Liquid Interfacial Polymerization: ANovel Catalyst for Synthesis of NH-1,2,3-Triazoles in PEG-400. Mater. Adv. 2021, 2, 21, 6996–7006

[30] Banu, A.; Khan, R.H.; Qashqoosha, M.T.A.; Manea, Y.K.; Furkan, M.; Naqyi S. Multi-spectroscopic and computational studies of interaction of bovine serum albumin, human serum albumin and bovine hemoglobin with bisacodyl, J.Nol.Struct., 2022, 1249, 131550.

[31] Rostamnezhad, F.; Fatemi, M.H. Comprehensive investigation of binding of some polycyclic aromatic hydrocarbons with bovine serum albumin: Spectroscopic and molecular docking studies, Bioorg. Chem., 2022, 120, 105656.

[32] Xu, C.; Gu, J.; Ma, X.; Dong, T.; Meng, X. Investigation on the interaction of pyrene with bovine serum albumin using spectroscopic methods, Spectrochim. Acta Part A: Mol. Biomol. Spectros., 2014, 125(5),391-195.